Atmospheric
Chemistry
and Physics

Experimental chemical budgets of OH, HO2, and RO2 radicals in rural air in western Germany during the JULIAC campaign 2019

Changmin Cho[1,a], Hendrik Fuchs[1], Andreas Hofzumahaus[1], Frank Holland[1], William J. Bloss[3], Birger Bohn[1], Hans-Peter Dorn[1], Marvin Glowania[1], Thorsten Hohaus[1], Lu Liu[1], Paul S. Monks[2], Doreen Niether[1], Franz Rohrer[1], Roberto Sommariva[2,3], Zhaofeng Tan[1], Ralf Tillmann[1], Astrid Kiendler-Scharr[1], Andreas Wahner[1], and Anna Novelli[1]

[1]Forschungszentrum Jülich, Institute of Energy and Climate Research, Troposphere (IEK-8), Jülich, Germany
[2]Department of Chemistry, University of Leicester, Leicester, UK
[3]School of Geography, Earth and Environmental Sciences, University of Birmingham, Birmingham, UK
[a]now at: School of Earth Sciences and Environmental Engineering, Gwangju Institute of Science and Technology (GIST), Gwangju, South Korea

Correspondence: Hendrik Fuchs (h.fuchs@fz-juelich.de) and Anna Novelli (a.novelli@fz-juelich.de)

Abstract. Photochemical processes in ambient air were studied using the atmospheric simulation chamber SAPHIR at Forschungszentrum Jülich, Germany. Ambient air was continuously drawn into the chamber through a 50 m high inlet line and passed through the chamber for 1 month in each season throughout 2019. The residence time of the air inside the chamber was about 1 h. As the research center is surrounded by a mixed deciduous forest and is located close to the city Jülich, the sampled air was influenced by both anthropogenic and biogenic emissions. Measurements of hydroxyl (OH), hydroperoxyl (HO2), and organic peroxy (RO2) radicals were achieved by a laser-induced fluorescence instrument. The radical measurements together with measurements of OH reactivity (k_{OH}, the inverse of the OH lifetime) and a comprehensive set of trace gas concentrations and aerosol properties allowed for the investigation of the seasonal and diurnal variation of radical production and destruction pathways. In spring and summer periods, median OH concentrations reached 6×10^6 cm^{-3} at noon, and median concentrations of both HO2 and RO2 radicals were 3×10^8 cm^{-3}. The measured OH reactivity was between 4 and 18 s^{-1} in both seasons. The total reaction rate of peroxy radicals with NO was found to be consistent with production rates of odd oxygen (O$_x$ = NO2 + O3) determined from NO2 and O3 concentration measurements. The chemical budgets of radicals were analyzed for the spring and summer seasons, when peroxy radical concentrations were above the detection limit. For most conditions, the concentrations of radicals were mainly sustained by the regeneration of OH via reactions of HO2 and RO2 radicals with nitric oxide (NO). The median diurnal profiles of the total radical production and destruction rates showed maxima between 3 and 6 ppbv h^{-1} for OH, HO2, and RO2. Total RO$_X$ (OH, HO2, and RO2) initiation and termination rates were below 3 ppbv h^{-1}. The highest OH radical turnover rate of 13 ppbv h^{-1} was observed during a high-temperature (max. 40 °C) period in August. In this period, the highest HO2, RO2, and RO$_X$ turnover rates were around 11, 10, and 4 ppbv h^{-1}, respectively. When NO mixing ratios were between 1 and 3 ppbv, OH and HO2 production and destruction rates were balanced, but unexplained RO2 and RO$_X$ production reactions with median rates of 2 and 0.4 ppbv h^{-1}, respectively, were required to balance their destruction. For NO mixing ratios above 3 ppbv, the peroxy radical reaction rates with NO were highly uncertain due to the low peroxy radical concentrations close to the limit of NO interferences in the HO2 and RO2 measurements. For NO mixing ratios below 1 ppbv, a missing source for OH and a missing sink for HO2 were found with maximum rates of 3.0 and 2.0 ppbv h^{-1}, respectively. The missing OH source likely consisted of a combination of a missing inter-radical HO2 to OH conversion reaction (up to

2 ppbv h^{-1}) and a missing primary radical source (0.5–1.4 ppbv h^{-1}). The dataset collected in this campaign allowed analyzing the potential impact of OH regeneration from RO$_2$ isomerization reactions from isoprene, HO$_2$ uptake on aerosol, and RO$_2$ production from chlorine chemistry on radical production and destruction rates. These processes were negligible for the chemical conditions encountered in this study.

1 Introduction

The hydroxyl (OH) radical is the dominant daytime atmospheric oxidant. It reacts with most trace gases in the troposphere and thereby controls the rate of their removal and chemical transformation. In the lower troposphere, OH is primarily produced by solar photolysis of ozone (O$_3$) and nitrous acid (HONO). The reaction of OH with trace gases leads to the formation of hydroperoxy (HO$_2$) or organic peroxy (RO$_2$, with $R =$ organic group) radicals, which undergo further radical reactions. Generally, these reactions are cyclic chain reactions, in which OH, HO$_2$, and RO$_2$ are converted into each other, while at the same time emitted pollutants are oxidized and converted into secondary pollutants such as ozone and oxygenated volatile organic compounds (OVOCs). Because the conversion of radicals occurs on a timescale of seconds to minutes, they are often referred to as the RO$_X$ family (OH + HO$_2$ + RO$_2$). The most important radical reactions in the lower atmosphere are summarized in Table 1. Understanding radical chemistry is the basis for reliable predictions of the atmospheric lifetime and chemical transformation of air pollutants and climate-relevant gases by atmospheric chemistry models (Stone et al., 2012).

The level of agreement between simulated and observed radical concentrations in various environments shows the degree of understanding of the underlying radical chemical mechanism. Even though good agreement is found in some cases (Tan et al., 2001; Konrad et al., 2003; Mihelcic et al., 2003; Lelieveld et al., 2008; Kubistin et al., 2010; Whalley et al., 2011), there are significant unexplained discrepancies between modeled and measured OH in forested regions (Wolfe et al., 2011; Griffith et al., 2013; Kim et al., 2013; Hens et al., 2013; Wolfe et al., 2014) and of HO$_2$ and RO$_2$ in polluted areas (Ren et al., 2003, 2006; Kanaya et al., 2007; Dusanter et al., 2009; Chen et al., 2010; Ren et al., 2013; Brune et al., 2016; Tan et al., 2018; Slater et al., 2020; Whalley et al., 2021), while different results are found depending on the abundance of nitric oxide (NO) in rural environments (Hofzumahaus et al., 2009; Lou et al., 2010; Elshorbany et al., 2012; Kanaya et al., 2012; Tan et al., 2017).

A chemical budget analysis using measured OH, HO$_2$, and RO$_2$ radical concentrations can help assess the strength of different radical production and loss paths. This allows identifying possible missing chemical processes by comparing the total production and destruction rates for the different radicals as concentrations are expected to be in steady state due to their short chemical lifetime. A large number of measurements needs to be available (e.g., OH reactivity, OH, peroxy radicals); therefore, there have only been a few studies focusing on the analysis of the chemical budget for OH radicals so far (Handisides et al., 2003; Hofzumahaus et al., 2009; Brune et al., 2016; Whalley et al., 2018; Tan et al., 2019; Whalley et al., 2021).

Results from field campaigns in China showed a larger OH radical destruction rate compared to its production rate in the afternoon, which points to an OH radical source that is unaccounted for. Discrepancies were highest when NO mixing ratios were lower than 2 ppbv (Hofzumahaus et al., 2009; Tan et al., 2019; Whalley et al., 2021). On the other hand, studies in urban areas in California (Brune et al., 2016) and in London (Whalley et al., 2018) as well as in a rural area in Hohenpeissenberg (Handisides et al., 2003) showed no significant gap between the OH production and destruction rates. Recently, radical measurements including RO$_2$ enabled the investigation of HO$_2$, RO$_2$, and RO$_X$ production and destruction rates in field campaigns in China (Tan et al., 2019; Whalley et al., 2021). Tan et al. (2019) showed that an RO$_2$ loss process was required in a campaign in Wangdu in summer, while HO$_2$ production and destruction rates were balanced. This suggests a missing conversion of RO$_2$ to OH in addition to the reaction of peroxy radicals with NO. Furthermore, Whalley et al. (2021) found large imbalances between peroxy radical production and destruction rates in Beijing, indicating substantially slower propagation of RO$_2$ to HO$_2$ radicals than anticipated.

In this study, OH, HO$_2$, and RO$_2$ radical concentrations as well as OH reactivity, the inverse of the OH radical lifetime, were measured in the atmospheric simulation chamber SAPHIR on the campus of Forschungszentrum Jülich (FZJ), Germany, in the Jülich Atmospheric Chemistry project (JULIAC) campaign. Ambient air was sampled from 50 m height into the SAPHIR chamber. From this dataset, a chemical budget analysis of OH, HO$_2$, RO$_2$ radicals, and their sum (RO$_X$) was done using measured concentrations allowing the investigation of whether all radical production and destruction processes were accounted for during spring and summer.

2 Methodology

2.1 JULIAC

The Jülich Atmospheric Chemistry (JULIAC) project campaign was conducted at Forschungszentrum Jülich (FZJ, 50.9° N, 6.4° E), Germany. The project consisted of four

1-month-long intensive campaigns studying atmospheric chemistry in ambient air in each season throughout 2019. The location is surrounded by a deciduous forest and is located in a rural environment near a town, Jülich (33 000 inhabitants), 25 km northeast, 40 km west, and 43 km southwest from the three large cities of Aachen, Cologne, and Düsseldorf, respectively. Therefore, ambient air is influenced by both biogenic and anthropogenic emission sources.

The investigation of the photochemistry was performed in the SAPHIR chamber, which was equipped with a large set of instruments measuring radicals, trace gases, and aerosol (Table 2). The SAPHIR chamber has a cylindrical shape and is made of a double-wall Teflon (FEP) film. A slight overpressure (35 Pa) is maintained in the chamber, and the space between the two films is permanently flushed with pure nitrogen (Linde, purity: $> 99 : 99990$ %) to prevent outside air from penetrating the inner chamber. The chamber is equipped with a shutter system allowing the air to be either shielded from or exposed to solar radiation.

In the JULIAC campaign, ambient air was sampled at a high flow rate of 660 m^3 h^{-1} from a 50 m high inlet line (104 mm inner diameter, SilcoNert$^{®}$ coated stainless steel) by means of an oil-free turbo blower (Aerzener Maschinenfabrik, AERZEN Turbo G3, type TB 50–0.6 S). Large particles (> 10 µm diameter) were removed by a SilcoNert$^{®}$-coated cyclone (LTG, ZSB-6). The temperatures in the inlet line and cyclone were controlled to be slightly higher than ambient temperature ($+1$ to 2 °C) to avoid water vapor condensation in the inlet system. A 3/2-way valve directed some of the air (flow rate of 250 m^3 h^{-1}) into the chamber. Two fans inside the chamber ensured fast mixing on a timescale of a few minutes. As a result, the chamber behaved as a continuously stirred photochemical flow reactor with a mean residence time of air of 1.1 h. During the transition time of 3.5 s from the tip of the inlet to the SAPHIR chamber, atmospheric RO$_X$ radicals are lost on walls, but concentrations are rapidly re-established in the sampled ambient air inside the sunlit chamber.

The use of the chamber as a flow reactor has advantages compared to field measurements in the open air. Perturbations of the studied chemistry due to local emissions of VOCs or NO$_x$ can be avoided. Transient fluctuations of reactants in the sampled air, for example due to spikes of NO from passing cars, are smoothed out in the chamber. Due to the homogeneous mixing, instruments connected to the chamber measure the same air composition, and segregation effects on reaction rates are insignificant.

The air composition could be influenced by the inlet line and chamber surfaces. As the whole inlet line is heated and chemically inert due to the SilcoNert$^{®}$ coating, no relevant wall loss or desorption of trace gases is expected from the inlet. This assumption was confirmed by comparing OH reactivity measured at several positions of the inlet line. No significant differences were found between measurements whether the air was sampled upstream of the cyclone or downstream of the blower. Wall losses of trace gases (VOCs, NO$_x$, O$_3$) inside the SAPHIR chamber were found to be negligible in previous experiments (e.g., Kaminski et al., 2017, Rolletter et al., 2020).

Nitrous acid (HONO) and formaldehyde (HCHO) are known to be emitted from the chamber film when it is exposed to solar radiation (Rohrer et al., 2005). These emissions significantly increase the concentrations of HONO and HCHO in the chamber. Due to the transmission through the Teflon film and shading from construction elements of the chamber, the absolute actinic flux density is reduced by 20 % to 40 % compared to outside the chamber. It is worth noting, however, that the relative spectral distribution of the solar radiation is not changed by the transmission through the chamber film (Bohn and Zilken, 2005).

The floor underneath the chamber is heated by the solar radiation. Although it is not in direct contact with the foil, the air temperature in the chamber was on average 0.7 °C higher during winter and autumn and 1.9 °C higher during spring and summer than the temperature outside the chamber in daytime. Since photochemistry was studied in the chamber, all data for chemical and physical conditions shown in this work refer to conditions inside the chamber.

The measurements in the campaign were interrupted at least once a week for calibration and maintenance of instruments. Some days were also excluded from the analysis in this work because the chamber shutter system was kept closed to protect the chamber film during bad weather from strong wind gusts and/or precipitation. Reference experiments with clean synthetic air were performed to investigate possible changes in the strength of chamber emissions and to check for instrumental backgrounds. In addition, chemical actinometry experiments, in which NO$_2$ was photolyzed in synthetic air, were performed before and after each intensive period. The comparison of actinometric and spectroradiometric j_{NO_2} values was used to track and correct for changes in light transmission due to aging of the chamber wall (Bohn et al., 2005).

2.2 Instrumentation

2.2.1 OH, HO$_2$, and RO$_2$ radical and OH reactivity (k_{OH}) measurements

OH, HO$_2$, and RO$_2$ radicals were measured by the FZJ laser-induced fluorescence (LIF) instrument, which included a newly developed chemical modulation reactor (CMR) for interference-corrected measurements of OH radicals (Cho et al., 2021). The signals of the instrument were calibrated against well-defined radical concentrations that were produced from water photolysis in synthetic air at a wavelength of 185 nm using radiation from a mercury lamp. A detailed description of the LIF instrument and its calibration can be found in previous publications (Holland et al., 2003; Fuchs et al., 2008, 2011, 2012).

Table 1. Chemical reactions and rate constants used for the analysis of the chemical budgets of radicals. Values of reaction rate constants are given for standard conditions (298 K, 1 atm). Actual numbers are used for the calculations.

Reaction		k(298 K, 1 atm) cm^{-3} s	k^a_{ERR}	Reference
Radical initiation reactions				
(R1)	HONO $+ h\nu \rightarrow$ OH $+$ NO	j^b_{HONO}		
(R2)	O$_3 + h\nu \rightarrow$ O^{1}D $+$ O$_2$	j^b_{O1D}		
(R2a)	O^{1}D $+$ H$_2$O $\rightarrow$ 2OH	2.1×10^{-10}	$\pm 13\%$	IUPAC
(R2b)	O^{1}D $+$ M $\rightarrow$ O^{3}P $+$ M	3.3×10^{-11}	$\pm 10\%$	IUPAC and JPL
(R3)	HCHO $+ h\nu \rightarrow$ 2HO$_2 +$ CO	j^b_{HCHO}		
(R4)	CH$_3$CHO $+ h\nu \rightarrow$ CH$_3$O$_2 +$ HO$_2 +$ CO	$j^b_{CH_3CHO}$		
(R5)	alkenes $+$ O$_3 \rightarrow$ OH, HO$_2$, RO$_2 +$ products			
(R5a)	propene $+$ O$_3 \rightarrow$ products^c	1.0×10^{-17}	$\pm 20\%$	IUPAC
(R5b)	cis-but-2-ene $+$ O$_3 \rightarrow$ product^d	1.3×10^{-16}	$\pm 12\%$	IUPAC
(R5c)	1-pentene $+$ O$_3 \rightarrow$ products^e	1.0×10^{-17}	$\pm 20\%$	MCMv3.3.1
(R5d)	2-hexene $+$ O$_3 \rightarrow$ products^f	1.1×10^{-17}	$\pm 20\%$	MCMv3.3.1
(R5e)	isoprene $+$ O$_3 \rightarrow$ products^g	1.3×10^{-17}	$\pm 10\%$	MCMv3.3.1
(R5f)	α-pinene $+$ O$_3 \rightarrow$ products^h	9.6×10^{-17}	$\pm 20\%$	IUPAC
Radical interconversion reactions				
(R6)	HCHO $+$ OH $+$ O$_2 \rightarrow$ CO $+$ H$_2$O $+$ HO$_2$	8.5×10^{-12}	$\pm 10\%$	IUPAC
(R7)	CO $+$ OH $+$ O$_2 \rightarrow$CO$_2 +$ HO$_2$	2.3×10^{-13}	$\pm 6\%$	IUPAC
(R8)	VOCs $+$ OH $+$ O$_2 \rightarrow$ RO$_2 +$ H$_2$O	j		
(R9)	RO$_2 +$ NO $\rightarrow$ products $+$ HO$_2 +$ NO$_2$	8.6×10^{-12}	$\pm 30\%$	Jenkin et al. (2019)
(R10)	HO$_2 +$ NO $\rightarrow$ OH $+$ NO$_2$	8.5×10^{-12}	$\pm 13\%$	IUPAC
(R11)	HO$_2 +$ O$_3 \rightarrow$ OH $+$ 2O$_2$	2.0×10^{-15}	$\pm 29\%$	IUPAC
Radical termination reactions				
(R12)	NO$_2 +$ OH $\rightarrow$ HNO$_3$	1.0×10^{-11}	$\pm 30\%$	IUPAC
(R13)	NO $+$ OH $\rightarrow$ HONO	9.7×10^{-12}	$\pm 13\%$	IUPAC
(R14)	RO$_2 +$ NO $\rightarrow$ RONO$_2$	4.6×10^{-13}	$\pm 30\%$	Jenkin et al. (2019)
(R15)	RO$_2 +$ RO$_2 \rightarrow$ products	3.5×10^{-13}	$\pm 50\%$	Jenkin et al. (2019)
(R16)	RO$_2 +$ HO$_2 \rightarrow$ ROOH $+$ O$_2$	2.3×10^{-11}	$\pm 50\%$	Jenkin et al. (2019)
(R17)	HO$_2 +$ HO$_2 \rightarrow$H$_2$O$_2 +$ O$_2$	$4.5 \times 10^{-12 i}$	$\pm 20\%$	IUPAC
Isoprene reactions				
(R18)	isoprene $+$ OH $\rightarrow$ products	1.0×10^{-10}	$\pm 8\%$	IUPAC
(R19)	isoprene–RO$_2$ (1,6-H shift) $\rightarrow$ products $+$ OH	0.01–0.06 s^{-1}		Peeters et al. (2014)
Cl reactions				
(R20)	ClNO$_2 +$ $h\nu \rightarrow$ Cl $+$ NO$_2$	$j^b_{ClNO_2}$		
(R21)	Cl$_2 +$ $h\nu \rightarrow$ 2Cl	$j^b_{Cl_2}$		
(R22)	VOCs $+$ Cl $\rightarrow$ RO$_2 +$ HCl	j		

^{a} 1σ uncertainty. ^{b} Measured photolysis frequencies. ^{c} Yield for OH: 0.36, HO$_2$: 0.10, RO$_2$: 0.42 from Novelli et al. (2021). ^{d} Yield for OH: 0.36, HO$_2$: 0.15, RO$_2$: 0.51 from Novelli et al. (2021). ^{e} Yield for OH: 0.32, HO$_2$: 0.09, RO$_2$: 0.37 from Novelli et al. (2021). ^{f} Yield for OH: 0.48, HO$_2$: 0.11, RO$_2$: 0.59 from Novelli et al. (2021). ^{g} Yield for OH: 0.26, HO$_2$: 0.26 from Malkin et al. (2010). ^{h} Yield for OH: 0.8 from Cox et al. (2020). ^{i} At 1% water vapor mixing ratio. ^{j} Highly variable depending on the specific VOC.

The OH radical is sampled through a nozzle with a 0.4 mm diameter pinhole and is excited by a pulsed laser at a wavelength of 308 nm in a low-pressure (4 hPa) fluorescence cell. The emitted resonant fluorescence is detected with a time delay by a time-gated micro-channel plate detector (MCP).

In the JULIAC campaign, a chemical modulation reactor (CMR) was implemented on top of the OH cell to quantify potential interferences. This is achieved by periodically removing ambient OH by an OH scavenger that is injected in the reactor (propane, Air Liquide, purity > 99.95 %,

Table 2. Specification of instruments used in the JULIAC campaign for the analysis in this work.

Species	Measurement technique	Time resolution	Limit of detection (1σ)	1σ accuracy
OH	LIF	270 s	0.7×10^6 cm^{-3}	18 %
OH	DOAS	134 s	0.8×10^6 cm^{-3}	6.5 %
HO$_2$	LIF	47 s	1×10^7 cm^{-3}	18 %
RO$_2$	LIF	47s	2×10^7 cm^{-3}	18 %
OH reactivity (k_{OH})	LP-LIF	180 s	0.2 s^{-1}	10 %
Photolysis frequencies	Spectroradiometer	60 s		18 %
O$_3$	UV photometry	60 s	0.5 ppbv	2 %
NO$_x$ (NO + NO$_2$)	Chemiluminescence*	60 s	NO: 20 pptv NO$_2$: 30 pptv	NO: 5 % NO$_2$: 7 %
CO, CO$_2$, CH$_4$, H$_2$O	Cavity ring-down spectroscopy	60 s	CO and CH$_4$: 1 ppbv CO$_2$: 25 ppbv H$_2$O: 0.1 %	5 %
HONO	LOPAP	180 s	5 pptv	10 %
HCHO	Cavity ring-down spectroscopy	300 s	0.1 ppbv	10 %
ClNO$_2$	I-CIMS	60 s	2.8 pptv	8.5 %
VOCs	PTR-TOF-MS VOCUS PTR-TOF-MS	30 s 30 s	15 pptv	14 %
Aerosol surface area	SMPS	7 min	10 nm – 1 µm	NA

* NO$_2$ was converted to NO before detection using a custom-built photolytic converter. NA: not available.

(5.0 ± 0.1) % mixture in nitrogen) before the air enters the fluorescence cell. During the campaign, the observed interference could be fully explained by the well-characterized interference from the photolysis of ozone in humid air inside the detection cell. No evidence for unexplained interference was found (Cho et al., 2021). The limit of detection for OH was 0.7×10^6 cm^{-3} and the accuracy was 18 % (1σ).

OH radical concentrations were also measured by differential optical absorption spectroscopy (DOAS) using a multiple folded light path for absorption inside along the chamber. The DOAS technique is a calibration-free technique (Hausmann et al., 1997; Schlosser et al., 2007, 2009). The limit of detection was 0.8×10^6 cm^{-3} and the 1σ accuracy was 6.5 %. Due to a technical laser problem, the DOAS instrument was not available in spring.

HO$_2$ radicals were detected by the LIF instrument in a separate detection cell, where HO$_2$ is chemically converted to OH radicals in the reaction with NO (Air Liquide, 1 % NO in N$_2$, purity > 99.5 %) that is injected in the fluorescence cell (Fuchs et al., 2011). During the JULIAC campaign, two different concentrations (2.5×10^{13} and 1.0×10^{14} cm^{-3}) of NO in the fluorescence cell were used to observe possible interference from specific RO$_2$ radicals as highlighted by Fuchs

et al. (2011). No difference between HO$_2$ measurements at high and low NO concentrations was found, suggesting that there was no significant interference from RO$_2$.

In addition, the sum of OH, HO$_2$, and RO$_2$ (RO$_X$) was measured by the RO$_X$–LIF system. Air is sampled into a chemical converter (pressure of ~ 25 hPa), where a mixture of NO (Air Liquide, 500 ppmv NO in N$_2$, purity > 99.5 %) and CO (Air Liquide, 10 % CO in N$_2$, purity > 99.997 %) is injected. The NO converts RO$_2$ radicals to HO$_2$ radicals, and CO converts OH radicals formed from the reaction of HO$_2$ radicals with NO back to HO$_2$. Therefore, an equilibrium between OH and HO$_2$ is established. Concentrations are chosen so that the equilibrium is on the side of HO$_2$. In a low-pressure cell downstream of the converter HO$_2$ radicals are converted to OH radicals by injecting excess NO (Air Liquide, pure NO, purity > 99.5 %) (Fuchs et al., 2008) that shifts the equilibrium between OH and HO$_2$ to OH. The RO$_2$ concentration is obtained from the difference between the sum measurement of RO$_X$ and measurements of OH and HO$_2$ concentrations in the other two detection cells. The RO$_2$ detection sensitivity was calibrated for methyl peroxy radicals (CH$_3$O$_2$), which are produced from the reaction of OH with methane (CH$_4$) in the calibration system. The resulting

calibration is also applicable to the majority of other atmospheric alkyl peroxy radicals (Fuchs et al., 2008, 2011), and recent laboratory tests performed with a variety of VOCs including monoterpenes and chained alkanes for the CO and NO mixing ratios applied in the RO$_X$ converter during the JULIAC campaign showed a decrease of less than 15 % sensitivity compared to methyl peroxy radicals, which is within the accuracy of the instrument.

The signals in the HO$_2$ and RO$_2$ detection systems contain a background signal observed when NO is injected into the detection cells, even if no radicals are present in the air sampled. The background signal can be characterized when the inlet of the detection system is overflown with synthetic air, which is part of the calibration procedures. During the JULIAC campaign the background varied from calibration to calibration and was often larger than the smallest signals measured in ambient air from the chamber (Table S1). The highest background signals obtained from calibrations are therefore regarded as an upper limit, and the variability is considered to be an additional uncertainty in the measured HO$_2$ and RO$_2$ concentrations. HO$_2$ and RO$_2$ background signals, which are subtracted in the evaluation of HO$_2$ and RO$_2$ measurements, were taken from reference experiments in the dark clean chamber, when no HO$_2$ or RO$_2$ radicals are expected. The subtracted signals for each period are available in Table S1 and in most cases were equivalent to concentrations lower than 1×10^7 cm^{-3} for both HO$_2$ and RO$_2$ measurements.

The total OH reactivity (k_{OH}), the inverse of the chemical lifetime of OH radicals, was measured in ambient air by a laser-flash photolysis LIF instrument (Lou et al., 2010; Fuchs et al., 2017). A high concentration of OH radicals is produced by flash photolysis (266 nm, 1 Hz repetition rate) of ozone in humid air (Reaction R2 in Table 1) in a flow tube that is on top of an OH fluorescence cell. The pseudo-first-order decay of OH in the chemical reactions with atmospheric reactants is measured, directly giving the OH reactivity.

2.2.2 Other trace gas, aerosol property, and photolysis frequency measurements

A comprehensive set of instruments operated during the JULIAC campaign (Table 2) analyzed the air composition inside the chamber. Photolysis frequencies inside the chamber were derived from solar actinic flux densities measured by a spectroradiometer mounted on the roof of the nearby institute building. Chamber values were calculated using a model approach considering shading effects and the influence of the chamber film (Bohn et al., 2005; Bohn and Zilken, 2005). Formaldehyde (HCHO) was detected by cavity ring-down spectroscopy (Picarro, G2307, Glowania et al., 2021). NO and NO$_2$ were measured by chemiluminescence (Eco Physics, TR780, NO$_2$ conversion by a custom-built photolytic converter). In addition, HONO was measured by long-path absorption photometry (LOPAP, Kleffmann et

al., 2006; Häseler et al., 2009), CO, CO$_2$, CH$_4$, and H$_2$O by cavity ring-down spectroscopy (Picarro, G2401), and O$_3$ by UV absorption (Ansyco-41M and Thermo scientific-49I). Volatile organic compounds (VOCs) were detected by a proton-transfer-reaction time-of-flight mass spectrometer (PTR-TOF-MS, Ionicon) (Jordan et al., 2009) and a VOCUS PTR-TOF-MS instrument (Aerodyne). The VOCs included in this study are listed in Table S2 and include isoprene and some carbonyl compounds. Total aerosol surface area was determined from measurements by a scanning mobility particle sizer (SMPS). In the summer and autumn periods, nitryl chloride (ClNO$_2$) was detected by a chemical ionization mass spectrometer using iodine as the reagent ion (I-CIMS) (Sommariva et al., 2018; Tan et al., 2022).

In addition to measurements in the chamber, concentrations of O$_3$ and NO$_x$ were also measured in the inlet system before the air flowed into the SAPHIR chamber. For these measurements, a combined system (Eco Physics, CraNO$_X$) consisting of an ozone photometer and a chemiluminescence instrument for NO$_x$ was deployed. Measurements were used to determine the photochemical ozone production in the JULIAC campaign. The measurement setup and concept of the evaluation will be discussed in detail in a further publication.

2.3 Chemical budget calculations

A chemical budget analysis, similar to that in Tan et al. (2019) and Whalley et al. (2021), was applied for OH, HO$_2$, RO$_2$, and the sum of all three radicals (RO$_X$) to the dataset from the JULIAC campaign. All reactions typically considered to be relevant for the generation and destruction of these radicals are considered (Table 1). Rate constants and their uncertainties were mainly taken from IUPAC recommendations (Atkinson et al., 2004, 2006; Cox et al., 2020) or more recent studies. If not otherwise specified, radical production and destruction rates are calculated from measured concentrations of reactants.

2.3.1 Chemical budget of OH radicals

The production rate of OH radicals includes primary production reactions (Reactions R1, R2, and R5) and radical inter-conversion reactions (Reactions R10 and R11):

$$P_{OH} = j_{HONO} [HONO] + \varphi_{OH} j_{O^1D} [O_3]$$
$$+ k_{10} [NO] [HO_2] + k_{11} [O_3] [HO_2]$$
$$+ \Sigma \left\{ \varphi_{OH}^i k_5^i [alkene]^i [O_3] \right\} + P_{OH, Isop.} \quad (1)$$

Here, φ_{OH} is the effective OH yield of the ozone photolysis including the reaction of excited oxygen atoms O(^{1}D) with H$_2$O, producing two OH radicals. φ_{OH}^i is the OH yield of the ozonolysis reaction of alkenes, and k_5^i represents the rate constants of the corresponding reactions.

$P_{OH, Isop}$ is the effective production of OH radicals from unimolecular reactions (1,6-hydrogen shift reactions) of

isoprene–RO$_2$ radicals (Z-δ-RO$_2$-I and II, Peeters et al., 2014) and the subsequent chemistry of products. As there was no measurement of speciated RO$_2$ radicals, isoprene–RO$_2$ radical concentrations are estimated from steady-state conditions considering their production from the reaction of isoprene with OH and their destruction in bimolecular reaction (reaction rate k_{bi}) as well as unimolecular reactions (bulk reaction rate $k_{\text{bulk 1,6-H}}$ as defined in Peeters et al., 2014).

$$\left[\text{RO}_2(\text{isop.})\right]_{\text{SS}} = \frac{k_{18}\left[\text{Isoprene}\right]\left[\text{OH}\right]}{k_{\text{bi}} + k_{\text{bulk 1,6-H}}} \quad (2)$$

$$k_{\text{bi}} = (k_9 + k_{14})\left[\text{NO}\right] + k_{15}\left[\text{RO}_2\right] + k_{16}\left[\text{HO}_2\right] \quad (3)$$

Bimolecular loss reactions include reactions with NO (Reactions R9 and R14), RO$_2$ (Reaction R15), and HO$_2$ (Reaction R16). The OH production from isoprene–RO$_2$ isomerization reactions is simplified in the calculation of the total OH production in this work by assuming that each isomerization reaction rapidly produces one OH radical from the subsequent reactions of products such as photolysis of hydroxy-peroxy aldehyde (HPALD). In this case, the radical production rate is equal to the loss rate of the isoprene–RO$_2$ due to isomerization reactions ($D_{Z-\delta-\text{RO}_2,\text{Isop.}}$).

$$P_{\text{OH,Isop.}} = D_{Z-\delta-\text{RO}_2,\text{Isop.}} = k_{\text{bulk 1,6-H}}\left[\text{RO}_2(\text{isop.})\right]_{\text{SS}} \quad (4)$$

The total loss rate of OH radicals for the chemical budget analysis is determined by the product of the total OH reactivity (k_{OH}) and the OH radical concentration.

$$D_{\text{OH}} = k_{\text{OH}}\left[\text{OH}\right] \quad (5)$$

2.3.2 Chemical budget of HO$_2$ radicals

The production rate of HO$_2$ radicals includes primary reactions (Reactions R3, R4, and R5) and interconversion reactions (Reactions R6, R7, and R9, Table 1).

$$\begin{aligned} P_{\text{HO}_2} &= 2j_{\text{HCHO}}\left[\text{HCHO}\right] + k_6\left[\text{HCHO}\right]\left[\text{OH}\right] \\ &\quad + k_7\left[\text{CO}\right]\left[\text{OH}\right] + k_9\left[\text{NO}\right]\left[\text{RO}_2\right] \\ &\quad + \Sigma\left\{\varphi^i_{\text{HO}_2}k^i_5[\text{alkene}]^i\left[\text{O}_3\right]\right\} \end{aligned} \quad (6)$$

Here, the photolysis frequency of HCHO (j_{HCHO}) includes only paths generating radicals. $\varphi^i_{\text{HO}_2}$ is the HO$_2$ yield from the ozonolysis of alkenes. The reactions of OH with H$_2$ and O$_3$ are not considered due to their negligible contributions to the HO$_2$ production.

The loss rate of HO$_2$ is determined by the reactions with NO (Reaction R10), O$_3$ (Reaction R11), RO$_2$ (Reaction R16), and HO$_2$ (Reaction R17).

$$\begin{aligned} D_{\text{HO}_2} &= \left(k_{10}\left[\text{NO}\right] + k_{11}\left[\text{O}_3\right] + k_{16}\left[\text{RO}_2\right]\right. \\ &\quad \left. + 2k_{17}\left[\text{HO}_2\right]\right)\left[\text{HO}_2\right] \end{aligned} \quad (7)$$

Here, the humidity dependence of k_{17} was taken into account. The reaction of HO$_2$ radicals with NO$_2$ is not included as the thermal decomposition of peroxynitric acid (HO$_2$NO$_2$) forming back HO$_2$ radicals and NO$_2$ is instantaneous for the temperatures experienced during the JULIAC campaign.

In a sensitivity calculation (Sect. 4.2.3), potential loss of HO$_2$ due to heterogeneous uptake on aerosol is investigated. The first-order loss rate ($k_{\text{het.}}$) can be described as

$$k_{\text{het.}} = \frac{\gamma_{\text{eff.}} \cdot \nu_{\text{HO}_2} \cdot [\text{AS}]}{4}, \quad (8)$$

where ν_{HO_2} is the mean molecular velocity of HO$_2$ ($4.44 \times 10^5 \, \text{cm s}^{-1}$ at 298 K), [AS] is the measured aerosol surface area concentration, and $\gamma_{\text{eff.}}$ is the effective uptake coefficient.

2.3.3 Chemical budget of RO$_2$ radicals

Primary sources of RO$_2$ radicals include all oxidation reactions of VOCs with OH, Cl, NO$_3$ radicals, and O$_3$. As the number of measured VOC species in this study was limited (Table S2) and because it is generally difficult to capture the entire spectrum of atmospheric VOCs (Goldstein and Galbally, 2007; Lou et al., 2010), the measured total OH reactivity (k_{OH}) can be used to calculate the RO$_2$ radical production from the reactions of VOCs with OH. First, the contributions from CO, NO, NO$_2$, HCHO, and O$_3$ are removed from the measured OH reactivity as these species do not form RO$_2$ radicals in the reaction with OH. It is then assumed that the remaining fraction can be attributed to organic compounds (VOC reactivity (k_{VOC})) including measured and unmeasured VOCs, which produce RO$_2$ radicals in their reaction with OH.

For some aromatics, such as toluene, benzene, and xylene, the prompt formation of HO$_2$ is expected from their reaction with OH (Nehr et al., 2011, 2014; Jenkin et al., 2019). However, in this campaign, their concentrations were small and their average contributions to the OH reactivity from VOCs were only 2.8 %. Therefore, their potential impacts on the RO$_2$ production are negligible (less than 1 %).

In addition, RO$_2$ production from ozonolysis needs to be included. In this work, only the reactions of measured organic compounds are considered. The contribution to the RO$_2$ production from the oxidation of VOCs by the NO$_3$ radical was negligible during daytime due to the low VOC load (low OH reactivity), so NO$_3$ destruction by photolysis and reaction with NO dominated.

Reactions of chloride (Cl) also produce RO$_2$ radicals, but the concentration was not measured in the JULIAC campaign. However, one of the most important precursor species, nitryl chloride (ClNO$_2$), was detected during the campaign (except in spring, Tan et al., 2022). ClNO$_2$ can accumulate during nighttime, but it is photolyzed after sunrise, yielding NO$_2$ and Cl atoms (Reaction R20). Assuming as an upper limit that each Cl atom reacts with a VOC (Tanaka et al.,

2003), the RO$_2$ production rate from Cl radicals can be calculated as

$$P_{RO_2,Cl} = j_{ClNO_2} [ClNO_2]. \tag{9}$$

The total RO$_2$ production rate is then calculated as

$$P_{RO_2} = k_{VOC} [OH] + \sum \left(\varphi_{RO_2}^i k_{R5}^i [alkene]^i [O_3] \right) + P_{RO_2,Cl}. \tag{10}$$

Here, $\varphi_{RO_2}^i$ is the RO$_2$ yield from the ozonolysis of alkenes species (Table 1).

With respect to the destruction rate of RO$_2$, its reactions with NO, HO$_2$, and other RO$_2$ as well as unimolecular reactions of specific isoprene–RO$_2$ radicals ($D_{Z-\delta-RO_2,Isop.}$) (Eq. 4) are considered in this work:

$$D_{RO_2} = \left((k_9 + k_{14}) [NO] + 2k_{15} [RO_2] \right.$$
$$\left. + k_{16} [HO_2] \right) [RO_2] + D_{Z-\delta-RO_2,Isop.} \tag{11}$$

2.3.4   Chemical budget of RO$_X$ radicals

In the chemical budget of the sum of OH, HO$_2$, and RO$_2$ (RO$_X$), inter-radical conversion reactions cancel out, and only initiation and termination reactions are included. Therefore, the RO$_X$ radical budget analysis allows investigating whether primary radical source reactions or termination processes are missing in the chemical mechanism used (Table 1).

The production rate of the RO$_X$ radicals is given by the sum of rates from radical initiation reactions (Reactions R1–R5, R20–R22, Table 1).

$$P_{RO_x} = j_{HONO} [HONO] + \varphi_{OH} j_{O^1D} [O_3]$$
$$+ 2 j_{HCHO} [HCHO]$$
$$+ \sum \left(\left(\varphi_{OH}^i + \varphi_{HO_2}^i + \varphi_{RO_2}^i \right) k_5^i [alkene]^i [O_3] \right)$$
$$+ P_{RO_2, Cl} \tag{12}$$

Radicals can additionally be produced from the photolysis of other oxygenated organic compounds (OVOCs, e.g., Reaction R4) not included in Eq. (12). Their potential impact is further discussed in Sect. 4.2.2.

The loss rate of the RO$_X$ radical is calculated by the sum of rates from radical termination reactions (Reactions R12–R17).

$$D_{RO_x} = (k_{13} [NO] + k_{12} [NO_2]) [OH] + k_{14} [NO] [RO_2]$$
$$+ 2k_{15} [RO_2]^2 + 2k_{16} [HO_2] [RO_2]$$
$$+ 2k_{17} [HO_2]^2 \tag{13}$$

2.3.5   Uncertainties in the calculated production and destruction rates

The uncertainty of each production or loss rate is calculated by Gaussian summation of the 1σ errors of the measured quantities (Table 2) and the uncertainties of the reaction rate constants (Table 1).

For reactions of RO$_2$ with NO (Reactions R9, R14), HO$_2$ (Reaction R16), and RO$_2$ (Reaction R15), generic rate constants are used for the sum of RO$_2$ radicals (Table 1, Jenkin et al., 2019). Rate constants of the NO reaction with RO$_2$ derived from hydrocarbons ($< C_5$) and with oxygenated peroxy radicals range from 7.7×10^{-12} to 1.1×10^{-11} cm^3 s^{-1} (Jenkin et al., 2019). The 1σ uncertainty of the rate constants varies from 6 % to 30 %. In the error calculations here, an upper limit value of 30 % is applied. However, for reactions of RO$_2$ with HO$_2$ and with RO$_2$, the range of rate constants varies by more than an order of magnitude. In the calculations, an uncertainty of 50 % is used for the reaction rate constants of RO$_2$ with HO$_2$ and with RO$_2$.

As there are no measurements of speciated RO$_2$ radicals, a yield of 5 % for the formation of organic nitrates is assumed for all RO$_2$, but the yield can vary between 1 % for methyl peroxy radicals (CH$_3$O$_2$) and more than 20 % for RO$_2$ from monoterpene species. This simplification can introduce systematic errors in the calculations (Sect. 4.2.1).

2.4   Odd oxygen production rate

In the troposphere, ozone is formed exclusively by the oxidation of NO to NO$_2$ through reaction with RO$_2$ (Reaction R9) and HO$_2$ (Reaction R10), followed by NO$_2$ photolysis (Fishman and Carney, 1984; Sillman et al., 1990; Kleinman et al., 2002).

During the day, the photolysis of NO$_2$ and the back reaction of NO with O$_3$ form a rapid photochemical equilibrium between O$_3$ and NO$_2$. The sum of O$_3$ and NO$_2$ is therefore defined as odd oxygen (O$_x$) (Han et al., 2011; Goldberg et al., 2015). The relative composition of O$_x$ depends on the NO$_2$ photolysis frequency and the NO concentration. For the conditions of the spring and summer periods in the JULIAC campaign, O$_x$ consisted predominantly (> 85 %) of O$_3$.

In this work, the net production rate of O$_x$ (P_{O_x}) was determined experimentally from the increase in O$_x$ in the sunlit SAPHIR chamber. Furthermore, measurements of radicals and NO$_x$ were used to calculate P_{O_x} from the rate of O$_x$ formation reactions (Reactions R9, R10) and O$_x$ loss by the reaction of NO$_2$ with OH (Reaction R12) (Mihelcic et al., 2003; Cazorla et al., 2012).

$$P_{O_X,net} = k_9 [NO] [RO_2] + k_{10} [NO] [HO_2]$$
$$- k_{12} [NO_2] [OH] \tag{14}$$

This calculation neglects minor O$_x$ destruction processes such as the reaction of O$_3$ with NO$_2$, OH, HO$_2$, Cl, or alkenes

since they did not play a notable role during the day in this campaign.

3 Results

3.1 Data quality of radical measurements

Performing measurements in the SAPHIR chamber allowed testing the accuracy of radical measurements in different ways that are typically not available in field experiments. First, OH radicals was measured by two independent instruments, the OH DOAS and LIF instruments (Cho et al., 2021). Second, the O$_x$ production rate calculated from measured concentrations of HO$_2$ and RO$_2$ could be compared to the observed increase in O$_x$ concentrations in the chamber, which can be solely attributed to chemical reactions. This is possible because other factors typically impacting the O$_x$ concentration in field experiments such as transportation processes are not effective.

OH concentrations were measured by the LIF instrument by applying the chemical modulation scheme and the DOAS in the winter, summer, and autumn periods of the campaign. As OH concentrations were close to the limit of detection in autumn and winter, a meaningful comparison of measurements was only possible for the summer period. A detailed comparison of measurements can be found in Cho et al. (2021). In general, the OH measurements of the two instruments agreed within their measurement errors (Table 1), giving a slope of 1.1 ± 0.02 in a linear regression analysis. The good agreement confirms that the newly developed chemical modulation system of the LIF instrument allowed for interference-free OH concentration measurements for conditions of the campaign. Only in the period from 22 to 26 August, which was characterized by exceptionally high temperatures (30 to 40 °C), were OH concentrations measured by the LIF instrument systematically higher by 25 % than those measured by the DOAS instrument for unknown reasons (Cho et al., 2021). OH concentrations measured by the DOAS instrument were used for the analysis of the radical budgets in this period.

Net O$_x$ production rates were determined from the measured increase in O$_x$ concentrations in the chamber and compared to calculations from the turnover rates of HO$_2$ and RO$_2$ reactions with NO. This calculation also takes the NO$_2$ loss due to its reaction with OH into account (Eq. 14). The odd oxygen production rate did not exceed 1 ppbv h^{-1} in winter and autumn due to the generally low photochemical activity in these seasons. In spring and summer, the O$_x$ production rate showed clear diurnal variations with noontime maxima that reached up to 16 ppbv h^{-1}. In these seasons, both methods for determining the O$_x$ production rate agreed within ± 15 % (1σ). Observed discrepancies were less than 1 ppbv h^{-1} when NO mixing ratios were lower than 1 ppbv but reached values of 3 ppbv h^{-1} for NO mixing ratios of 3–4 ppbv NO. The largest discrepancy of 8.5 ppbv h^{-1} was found in the morning on 29 April, when the NO mixing ratio exceeded 9 ppbv. High NO values suppressed HO$_2$ and RO$_2$ concentrations to values below 2.0×10^7 cm^{-3}, which is within the range of the background corrections for the HO$_2$ and RO$_2$ measurements (Table S1). Under these conditions, an erroneous background subtraction may have caused the observed discrepancies.

3.2 Meteorological and chemical conditions during the JULIAC campaign

A broad range of meteorological and chemical conditions was encountered during the JULIAC campaign. During the winter and autumn periods (Figs. S1 and S2), the sky was often overcast and it rained frequently. Temperatures were generally below 10 °C and the photolysis frequencies of ozone (j_{O_1D}) and nitrogen dioxide (j_{NO_2}) mostly remained below 1.5×10^{-6} and 2×10^{-3} s^{-1}, respectively. During spring and summer, temperatures in the chamber were up to 35 °C in mid-April and 40 °C between 24 and 31 August (Figs. 1 and 2). Photolysis frequencies in the chamber were 1×10^{-5} s^{-1} (j_{O_1D}) and 4×10^{-3} s^{-1} (j_{NO_2}).

The air was sampled at all times from 50 m above the ground. The temperature at different heights measured between 5 m and 120 m at a meteorological tower near the SAPHIR chamber showed that the air was well mixed within this height range during the day. Therefore, it can be assumed that the chemical composition of the air sampled into the chamber is representative of the air within the atmospheric boundary layer. At night, vertical temperature profiles showed atmospheric stratification below 100 m. The air at 50 m can be assumed to be isolated from the ground and therefore not affected by surface emissions or deposition on surfaces at the ground level.

Overall, relatively clean air was sampled during the whole of the JULIAC campaign, as indicated by CO and NO mixing ratios below 0.3 ppmv and 2 ppbv, respectively. Concentrations of anthropogenic organic compounds (e.g., benzene and toluene) were low with mixing ratios of less than 0.5 ppbv. Even though the measurement site is surrounded by a deciduous forest, the concentrations of biogenic organic compounds such as isoprene and monoterpenes were also low (median 0.8 ppbv and 0.15 ppbv, respectively) compared to previously reported values measured on the campus of FZJ in summer, when isoprene concentrations ranged between 0.5 and 4 ppbv (Komenda et al., 2003; Spirig et al., 2005; Kanaya et al., 2012). A possible reason for the low values could be damage to trees from severe droughts in the previous year (BMEL, 2021).
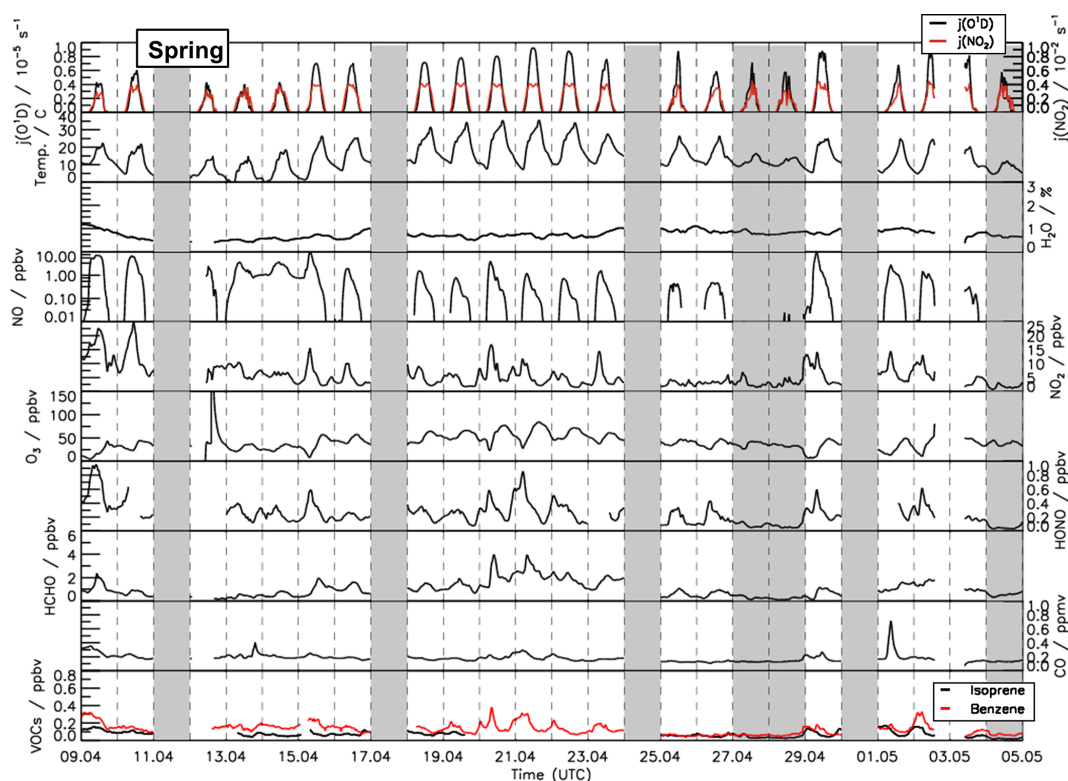
Figure 1. Time series of temperature and trace gas concentrations during the spring period of the JULIAC campaign. Vertical dashed lines denote midnight. Grey shaded areas indicate calibration days when no measurements were done and days when the chamber roof was closed due to bad weather conditions.

3.3 OH, HO$_2$, and RO$_2$ radical concentrations and OH reactivity during the winter and autumn periods of the JULIAC campaign

During winter (Fig. S3) and autumn (Fig. S4), daytime OH radical concentrations were below 1×10^6 cm^{-3}, mainly due to low primary radical production. Daytime peroxy radical (HO$_2$ and RO$_2$) concentrations during these periods were also very low with average values below 2×10^7 cm^{-3} (Fig. S5), which is close to the limit of detection of RO$_2$ radicals (Table 2) and within the uncertainty of the background corrections for HO$_2$ and RO$_2$ (Table S1). During winter and autumn, HO$_2$ concentrations typically increased in the morning and reached peak concentrations of 2×10^7 cm^{-3} at noon. Concentrations decreased in the evening and night with minimum values right before sunrise. In contrast, nighttime RO$_2$ concentrations increased to values between 3 and 4×10^7 cm^{-3} after sunset, when the chemical loss due to their reaction with NO became negligible, while RO$_2$ radicals were still produced from reactions of VOCs with NO$_3$ and O$_3$. NO concentrations were essentially zero at that time because NO production by the photolysis of NO$_2$ stopped and NO rapidly reacted with ozone. RO$_2$ radical concentrations decreased in the morning to values that were similar to those of HO$_2$ radicals as can be expected for conditions with

high NO mixing ratios, which led to a fast loss of RO$_2$ and HO$_2$ in their reactions with NO.

The measured OH reactivity (k_{OH}) ranged between 4 and 33 s^{-1} during winter and autumn periods. The highest value was observed on 21 January, when a highly polluted plume containing 50 ppbv of NO was sampled.

The measured OH reactivity can be compared to OH reactivity calculated by summing up the product between measured OH reactant concentrations and their reaction rate constants with the OH radical. On average, 1.3 s^{-1} (18 %) of the measured OH reactivity could not be explained by the measured OH reactants during the winter and autumn periods (Fig. S5). NO$_x$, CH$_4$, CO, and VOCs contributed approximately 43 %, 3 %, 20 %, and 13 %, respectively, to the measured OH reactivity.

3.4 OH, HO$_2$, and RO$_2$ radical concentrations and OH reactivity during the spring and summer periods of the JULIAC campaign

During spring and summer (Figs. 3, 4 and 5), maximum daytime OH concentrations were between 6 and 8×10^6 cm^{-3}. The highest OH concentration (1.2×10^7 cm^{-3}) occurred on 31 August. The diurnal OH concentration profile shows a high correlation with the ozone photolysis frequency (j_{O^1D})
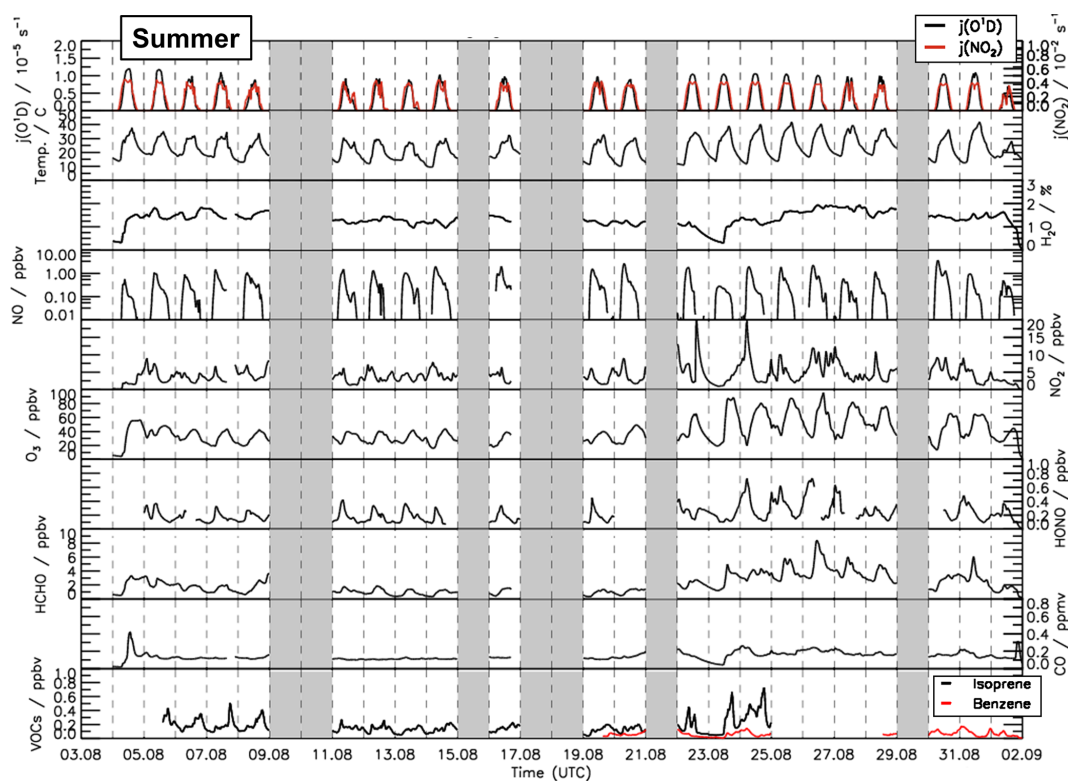
Figure 2. Time series of temperature and trace gas concentrations during the summer period of the JULIAC campaign. Vertical dashed lines denote midnight. Grey shaded areas indicate calibration days when no measurements were done and days when the chamber roof was closed due to bad weather conditions.

as observed in previous field campaigns (e.g., Ehhalt and Rohrer, 2000; Handisides et al., 2003; Holland et al., 2003).

Unfortunately, the measurements of HO$_2$ and RO$_2$ radicals were not available for the first 2 weeks of the spring campaign due to a malfunction of the instrument. Daily maximum HO$_2$ and RO$_2$ concentrations were in the range of 2 to 4×10^8 cm^{-3} during the spring period and the first half of the summer period. Maximum HO$_2$ and RO$_2$ concentrations were 8.0×10^8 and 7.0×10^8 cm^{-3}, respectively, during the second half of summer period. In spring and summer, peroxy radical concentrations showed a distinct diurnal pattern. Both HO$_2$ and RO$_2$ radical concentrations were suppressed in the early morning (between 04:00 and 07:00 UTC) due to the reaction with elevated NO mixing ratios of up to 1.5 ppbv. Maximum peroxy radical concentrations were usually reached in the afternoon ($\sim$ 14:00), when NO concentrations were lowest.

The measured OH reactivity values were in the range of 4 to 18 s^{-1}. High values were observed between 23 and 31 August due to high emissions of biogenic volatile organic compounds (BVOCs) from plants at high ambient temperatures. The OH reactivity that cannot be attributed to the measured OH reactants was on average 2.5 s^{-1} (40 %), which is much higher than observed in the winter and autumn periods (Fig. S5). CO and CH$_4$ contributed 10 % and 4 %, respec-

tively. Due to the high emissions of biogenic organic compounds in spring and summer, the attributed contribution of organic compounds to the total measured OH reactivity was 20 % and the contribution of NO$_x$ was only 19 %, which is much less compared to the winter and autumn periods. Isoprene had the largest contribution among all VOCs, accounting for up to 5 % of the total measured OH reactivity. Unfortunately, the number of detected VOC species in the JULIAC campaign was small (Table S2).

In the JULIAC campaign, nighttime OH concentrations were clearly below the limit of detection of the FZJ CMR–LIF instrument (0.7×10^6 cm^{-3}). When all nighttime data are averaged, mean OH concentrations with 1σ standard errors of $(3 \pm 1) \times 10^4$ and $(5 \pm 3) \times 10^4$ cm^{-3} are obtained for the spring and summer periods, respectively. These low values support the absence of instrumentally produced OH and indicate very low nocturnal OH production at 50 m height in the absence of NO and solar UV.

3.5 Chemical budgets of OH, HO$_2$, RO$_2$, and RO$_X$ radicals in the spring and summer periods

Due to the very low photochemical activity observed in autumn and winter, which resulted in radical concentrations close to the detection limit of the instrument, the chemical
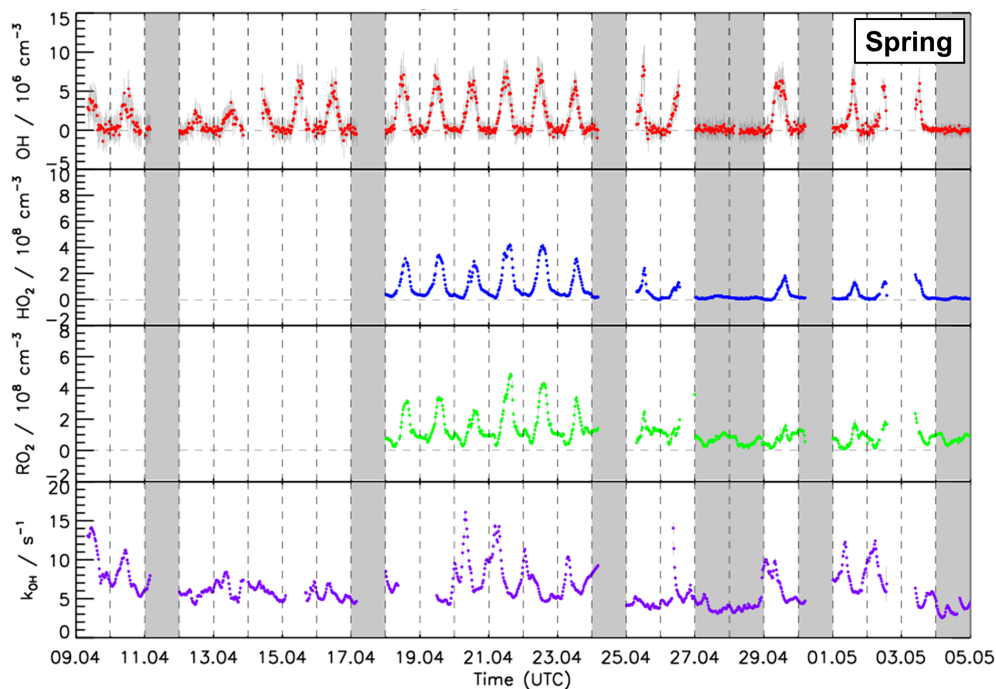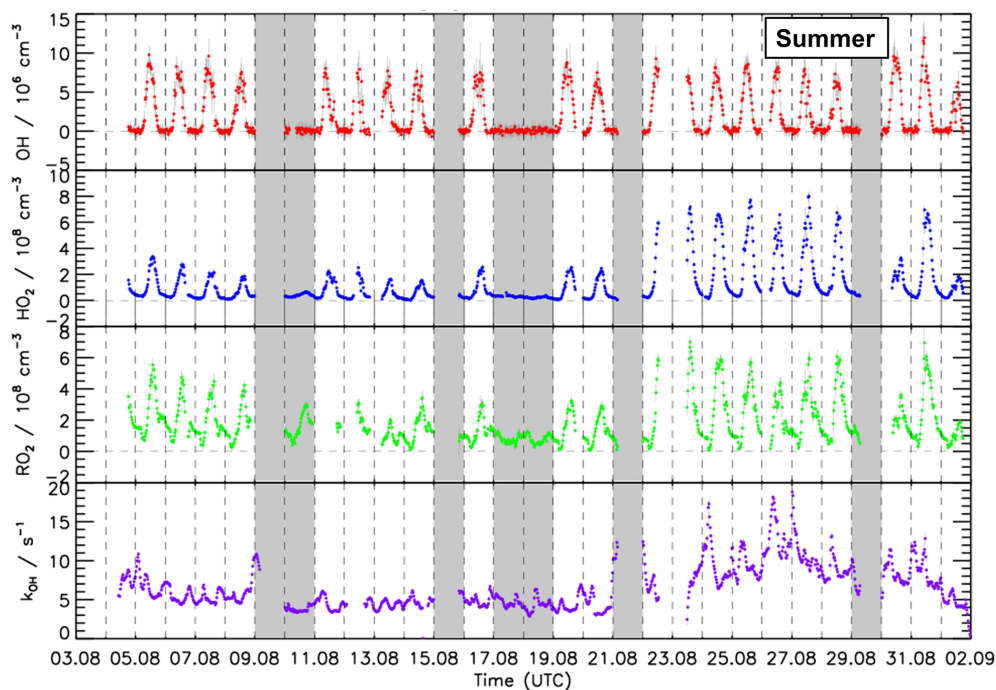
Figure 3. Time series of OH, HO$_2$, and RO$_2$ radical concentration measured by the FZJ LIF–CMR instrument and measurements of the OH reactivity (k_{OH}) measured in the spring period of the JULIAC campaign (Cho et al., 2022). Vertical bars represent 1σ statistical errors. Vertical dashed lines denote midnight. Grey shaded areas indicate calibration days when no measurements were done and days when the chamber roof was closed due to bad weather conditions.

Figure 4. Time series of OH, HO$_2$, and RO$_2$ concentration measured by the FZJ LIF–CMR instrument and measurements of the OH reactivity (k_{OH}) in the summer period of the JULIAC campaign (Cho et al., 2022). Vertical bars represent 1σ statistical errors. Vertical dashed lines denote midnight. Grey shaded areas indicate calibration days when no measurements were done and days when the chamber roof was closed due to bad weather conditions.
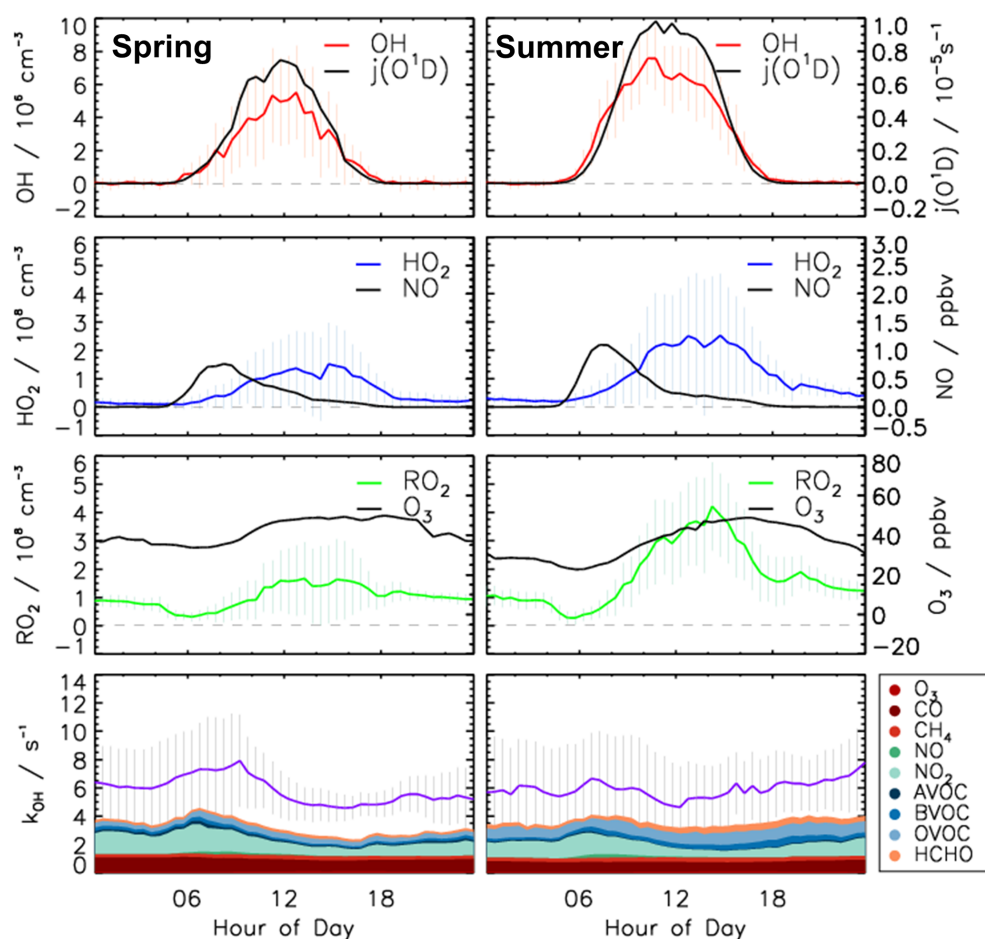
Figure 5. Median values of the diurnal profiles of OH, HO₂, RO₂, k_{OH}, j_{O_1D}, NO, and O₃ measured in the spring and summer periods of the JULIAC campaign. Colored areas represent the contributions of measured reactants to the total OH reactivity. Vertical lines give 25th and 75th percentile values.

budget analysis is only discussed for data from the spring and summer periods. It focuses on daytime conditions.

Time series of turnover rates of reactions involving OH, HO₂, RO₂, and RO$_X$ radicals in the spring and summer periods are presented in Figs. 6 and 7, respectively, and median diurnal profiles in Fig. 8. Typical daytime turnover rates of OH, HO₂, and RO₂ radicals were between 3 and 10 ppbv h⁻¹. The rates of RO$_X$ production and destruction ranged from 1 to 3 ppbv h⁻¹, which is 2 to 4 times lower than those of OH, HO₂, and RO₂ because radical conversion reactions cancel out. The highest OH turnover rate of 13 ppbv h⁻¹ was observed on 31 August, when the air temperature in the chamber reached up to 40 °C. Unusually high turnover rates for HO₂, RO₂, and RO$_X$ radicals occurred on 29 April with values of 14, 15, and 4 ppbv h⁻¹, respectively, when the NO mixing ratio exceeded 9 ppbv. For the reasons stated in Sect. 3.1, the HO₂ and RO₂ data on this date are considered highly uncertain and were excluded from further analysis of the chemical budgets.

Diurnal variations of total radical production and destruction rates, as well as of the contributions of the most important reactions, are shown as median values for the entire spring and summer period in Fig. 8. For OH, the reaction of HO₂ with NO (Reaction R10) was the dominant production pathway, contributing more than 70 % to the total production rate in both spring and summer periods. The photolysis of HONO (Reaction R1) was the most important primary OH source during daytime, contributing approximately 20 % to the total OH production. The reaction of HO₂ with ozone (Reaction R11), the photolysis of ozone (Reaction R2), and the ozonolysis of alkenes (Reaction R5) contributed less than 3 % to the total OH production. The maximum median total OH production rate of 3.5 ppbv h⁻¹ was observed in the morning shortly after the peak NO concentration in both spring and summer (Fig. 5). Values gradually decreased until sunset. Median total OH destruction rates were higher than production rates and reached up to 5 and 6 ppbv h⁻¹ at noon in spring and summer, respectively. The contributions of different reactions to the total OH destruction rate
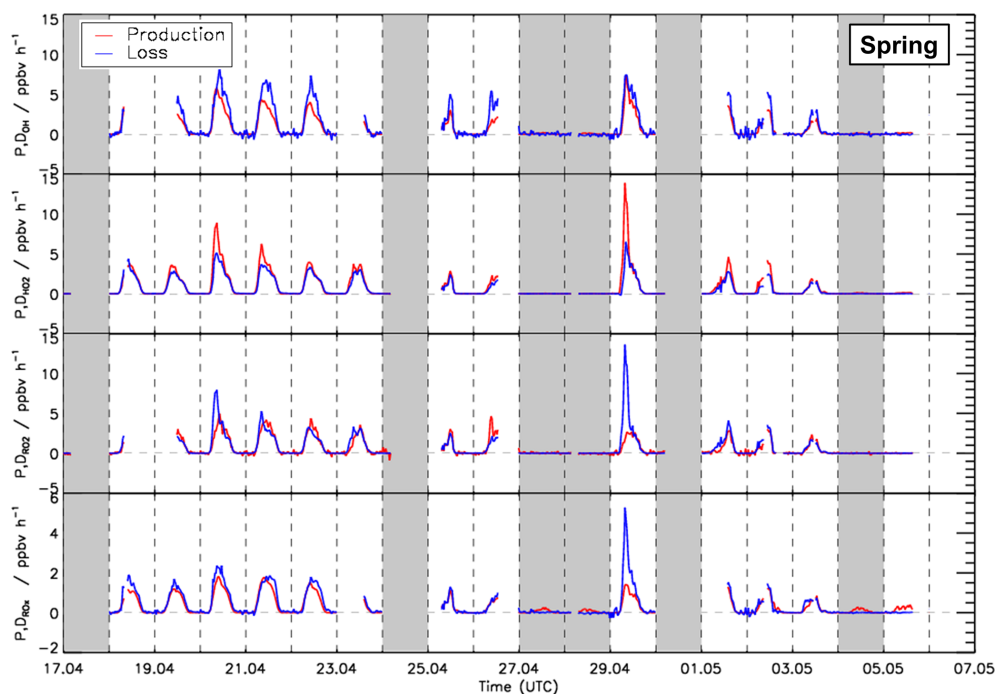
Figure 6. Time series of total production and destruction rates of OH, HO$_2$, RO$_2$, and RO$_X$ radicals in the spring period of the JULIAC campaign. Vertical dashed lines denote midnight. Grey areas indicate calibration days and days when the chamber roof was closed.
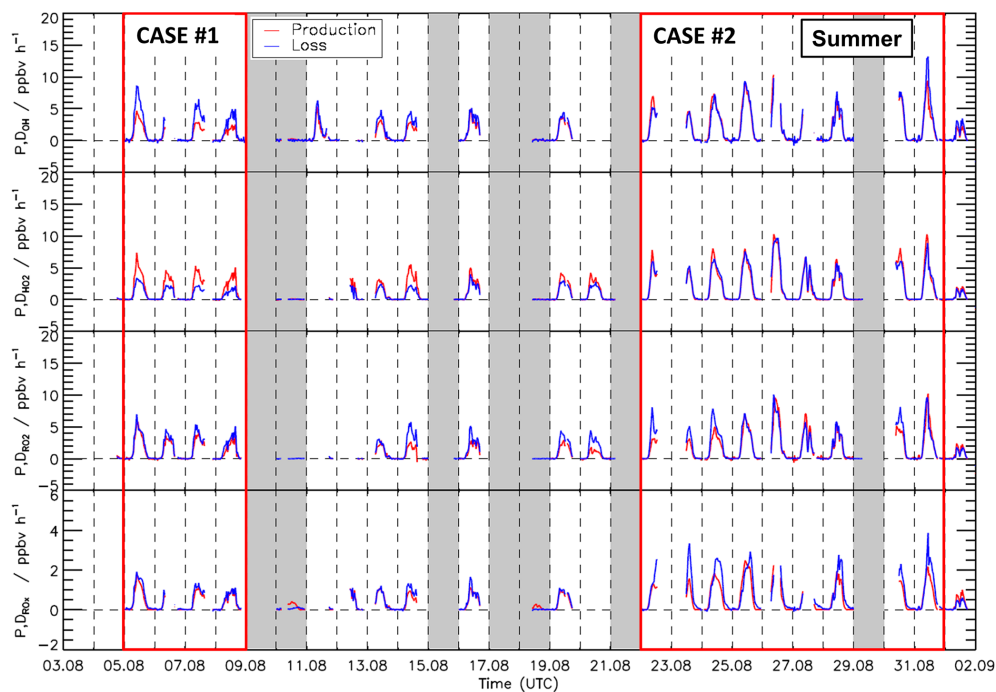

Figure 7. Time series of total production and destruction rates of OH, HO$_2$, RO$_2$, and RO$_X$ radicals in the summer period of the JULIAC campaign. Vertical dashed lines denote midnight. Grey areas indicate calibration days and days when the chamber roof was closed. The red boxes denote periods that are discussed in more detail (Case 1 and Case 2).

are described by the contribution of OH reactants to the OH reactivity (Sect. 3.4, Fig. 5).

Short-lived radicals are expected to be in a steady state, and therefore radical production and destruction rates must be balanced. An imbalance between the calculated rates indicates inaccurate data or a missing radical production or destruction process. The daily peak of the OH production rates was typically lower than the destruction rate by approximately 1.8 ppbv h^{-1} in the spring and 2.5 ppbv h^{-1} in the summer period (36 % and 43 % of the total OH destruction rate). These discrepancies are higher than the uncertainty of the calculation (Fig. 8).

80 % of the HO$_2$ production rate consisted of the reaction of RO$_2$ with NO (Reaction R9). The remaining part of the HO$_2$ production rate was due to the photolysis of formaldehyde (9 %) and the reaction of formaldehyde with OH (10 %). Other reactions producing HO$_2$ played a minor role (<1 %). The HO$_2$ destruction was mostly due to the reaction of HO$_2$ with NO (Reaction R10), contributing on average 88 % to the total production rate. The loss due to reaction of HO$_2$ with RO$_2$ radicals (Reaction R16) contributed on average 9 % to the total loss.

Median values of the total HO$_2$ destruction and production rates were well balanced in the spring period, with the production rate being slightly higher than the destruction rate. The maximum difference of 1 ppbv h^{-1}, however, was insignificant compared to the uncertainty of the calculation. A similar tendency but more pronounced feature was observed in summer. Here, the median value of the production rate was higher than that of the destruction rate by 1.8 ppbv h^{-1} (38 % of the total HO$_2$ production rate), but differences were variable (Fig. 7). This aspect is discussed in more detail for two periods (Sect. 3.7 and 3.8), which exhibited different degrees of imbalance in the radical budgets.

The RO$_2$ production rate was dominated by the reaction of VOCs with OH (Reaction R8). The contributions of ozonolysis of measured alkenes to the RO$_2$ production were very small (less than 1 %). The reaction of RO$_2$ with NO (Reaction R9) dominated the RO$_2$ destruction and contributed more than 90 % to the total loss rate. In the late afternoon, the RO$_2$ termination reaction with HO$_2$ gained importance with contributions of up to 10 %. Although slight imbalances of up to 1 ppbv were observed in the early morning, the RO$_2$ production and destruction rates were generally balanced within the uncertainty of calculations in both spring and summer.

Figure 9 shows the calculated RO$_X$ production and destruction rates. The photolysis of HONO (Reaction R1), HCHO (Reaction R3), and O$_3$ (Reaction R2) was the dominant process initiating radical chemistry and contributed 45 %, 38 %, and 15 %, respectively, to the total RO$_X$ production rate on average in both periods. In the morning, the reaction of OH with NO$_2$ (Reaction R12) was the most important radical termination process, contributing up to 65 % to the total RO$_X$ destruction rate. In addition, due to relatively high NO mixing ratios in the early morning, the re-
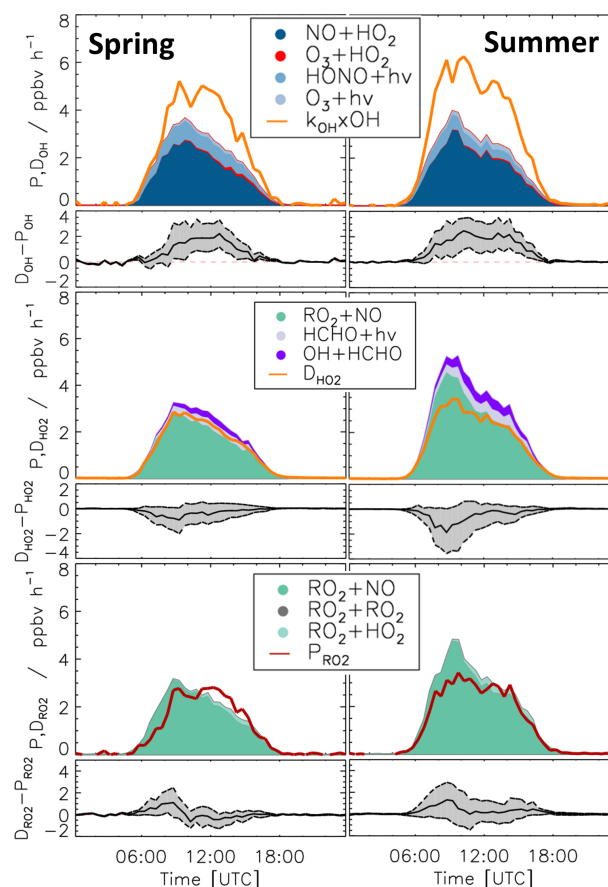

Figure 8. Median values of production and destruction rates of OH, HO$_2$, and RO$_2$ radicals in the spring and summer periods of the JULIAC campaign, with data from 29 April excluded. In addition, the differences between the destruction and production rates are shown. Grey areas indicate the 1σ uncertainty derived from experimental errors of the measured quantities (Table 2) and of the reaction rate constants (Table 1). The reactions that have insignificant contributions to the production or destruction rates are not shown.

actions of OH with NO (Reaction R13) and RO$_2$ with NO, which yields organic nitrate (Reaction R14), were also significant radical termination processes, contributing 13 % and 17 % to the total RO$_X$ destruction rate, respectively. In the afternoon, radical self-reactions (Reactions R15–R17) and, in particular, the reaction of RO$_2$ with HO$_2$ (Reaction R16) dominated the RO$_X$ destruction due to the low NO and NO$_2$ mixing ratios. In both the spring and summer periods, the total RO$_X$ destruction rate was slightly higher than the production rate, in particular in the afternoon. The imbalance was up to 0.5 ppbv h^{-1}, which is higher than the uncertainty of the calculations.

Meteorological and chemical conditions were variable, especially in the summer period, causing variations in the balance between radical production and destruction rates (Fig. 7 and Table S3). In the following, the chemical budgets with
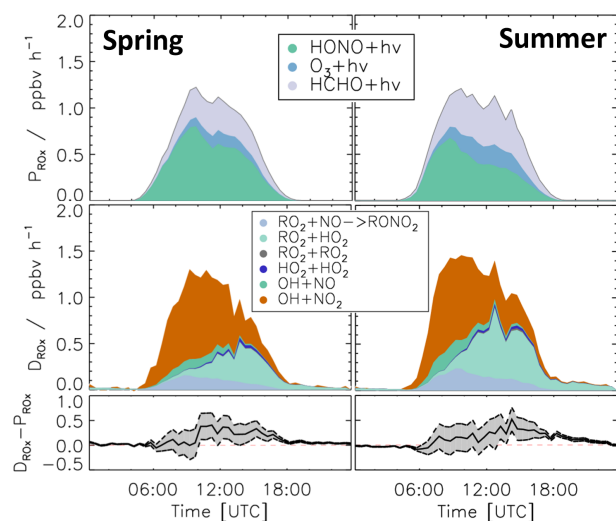
Figure 9. Median values of production and destruction rates of RO_X radicals during the spring and summer periods of the JULIAC campaign. In addition, the differences between the destruction and production rates are shown. Grey areas indicate the 1σ uncertainty derived from experimental errors of the measured quantities (Table 2) and of the reaction rate constants (Table 1). The reactions that have insignificant contributions to the production or destruction rates are not shown.

the largest and smallest observed imbalances are discussed: 5–8 August (Case 1) and 22–31 August (Case 2).

3.5.1   Case 1: 5–8 August 2019

For the period between 5 and 8 August, relatively low NO mixing ratios (maximum: 1 ppbv, median: 0.26 ppbv) and typical summer temperatures for this region (median: 27 °C) were observed (Fig. 10 and Table S3).

As for the whole summer period (Fig. 8), the reactions of peroxy radicals with NO (Reactions R9, R10) dominated the inter-radical conversion reactions of OH, HO₂, and RO₂ in this period (Fig. 10). A significant imbalance between the OH production and destruction rates of up to 3.0 ppbv h⁻¹ (51 % of the total OH destruction rate) is found, which cannot be explained by the uncertainty of the calculations. The total HO₂ production rate was 2.0 ppbv h⁻¹ higher than the destruction rate (48 % of the total HO₂ production rate), whilst the RO₂ production and destruction rates were well balanced. Relatively small but nevertheless significant differences between RO_X production and destruction rates (0.5 ppbv h⁻¹) were observed during daytime (Fig. 11).

3.5.2   Case 2: 22–31 August 2019

During the period from 22 to 31 August, the temperature was generally high and reached a maximum value of 42 °C inside the chamber. The concentrations of the radical precursors (HONO, HCHO, and O₃) were higher than those observed

in Case 1 (Table S3). Ozone mixing ratios reached values up to 100 ppbv, while daytime NO mixing ratios were similar as in Case 1 (<1.5 ppbv, median value of 0.22 ppbv). The conditions outside the chamber were characterized by stagnant air (wind speed <4 m s⁻¹ at 50 m height) with no precipitation. At these conditions, vigorous biogenic emissions can be expected (Vilà-Guerau de Arellano et al., 2009; Sarkar et al., 2020). Enhanced biogenic VOC emissions and their photochemical degradation can therefore explain the higher VOC and HCHO concentrations in Case 2 compared to the cooler period at the beginning of the month (Table S3). The larger VOC reactivity and comparable OH concentrations resulted in HO₂ and RO₂ concentrations that were approximately 2 to 3 times higher than in Case 1 (Table S3).

Imbalances between the radical production and destruction rates were a factor of 2 smaller in the warmer and more photochemically active period of Case 2 compared to Case 1. OH destruction rates were up to 1.5 ppbv h⁻¹ (25 % of the total OH destruction rate) higher than the total production rate (Fig. 10). The HO₂ production and destruction rates agree within ± 1 ppbv h⁻¹. The contributions from photolysis of HCHO and the reaction of HCHO with OH to the HO₂ production rate were larger compared to other periods with values of up to 15 % and 13 %, respectively, due to high HCHO mixing ratios of up to 8 ppbv (Fig. 2). The RO₂ production and destruction rates showed imbalances up to 1.5 ppbv h⁻¹ in the late afternoon.

While HONO photolysis was the dominating RO_X source most of the time in spring and summer (Fig. 9), HO₂ production from the photolysis of HCHO was the most important primary radical source in Case 2 due to the high concentration of HCHO (Fig. 11). Although the chemical budgets for each radical species were essentially closed within the experimental uncertainty, the total loss rate of RO_X was consistently higher than the production rate during daytime. The deviation was higher than the experimental uncertainty and reached a maximum value of 1.4 ppbv h⁻¹ at noontime.

3.5.3   NO dependence of radical production and destruction rates

One of the most influential parameters for the radical chemistry is the concentration of NO, since the reaction with NO dominates the conversion rate of RO₂ to HO₂ (Reaction R10) and HO₂ to OH (Reaction R9) (Fig. 10). Figure 12 shows the NO dependence of median values of the calculated production and destruction rates for the different radicals for the spring and summer period.

For OH, the production rates are consistently lower than the destruction rates by about 1.5 ppbv h⁻¹ for NO mixing ratios lower than 1 ppbv NO. At higher NO, the OH budget is balanced within the experimental uncertainty. For HO₂, an inverse pattern is observed. Below 1 ppbv NO, the production rate is higher than the destruction rate by about 1 ppbv h⁻¹. Only for lowest NO mixing ratios are the production and de-
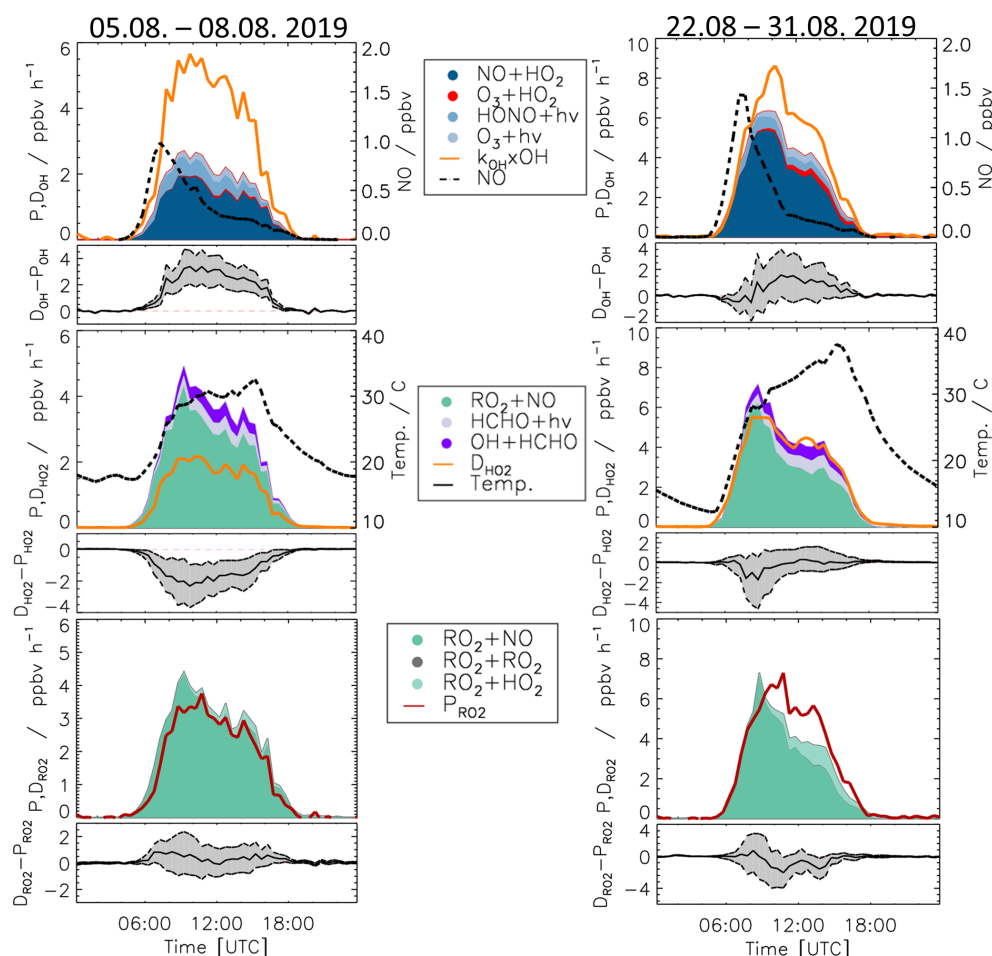
Figure 10. Production and destruction rates of OH, HO$_2$, and RO$_2$ radicals for Case 1 (5–8 August 2019) and Case 2 (22–31 August 2019). In addition, the differences between the destruction and production rates are shown. Grey areas give the 1σ uncertainty derived from experimental errors of the measured quantities (Table 2) and of the reaction rate constants (Table 1). The reactions that have insignificant contributions to the production or destruction rates are not shown.

struction rates balanced. For NO mixing ratios above 1 ppbv, the chemical budget of HO$_2$ is essentially closed. For NO mixing ratios of 3.5 ppbv, the difference between the production and destruction rate is noticeably high (more than 4 ppbv h^{-1}) but also has large uncertainty. For RO$_2$ radicals, the chemical budget is closed for NO mixing ratios below 1 ppbv, but an increasing discrepancy between the loss and production rates is observed with increasing NO mixing ratios. While the production rate is relatively constant at a value of 2.5 ppbv h^{-1}, the loss rate increases to values of up to 7.5 ppbv h^{-1} at 3.5 ppbv NO. The budget of RO$_X$, in which radical interconversion reactions cancel out, is mostly balanced over the whole range of NO. Only for the lowest and highest NO mixing ratios is the destruction rate 0.6 ppbv h^{-1} higher than the production rate.

4 Discussion

4.1 Discrepancies in the chemical budgets of radicals

The highest imbalances in the chemical budgets of radicals are found for OH radicals. In spring and summer, their production rate was consistently lower than the loss rate (Fig. 8). This deficit was largest at the beginning of August (Case 1, Fig. 10) when the discrepancy reached (3.0 $\pm$ 1) ppbv h^{-1}.

Imbalances in the radical budgets can be observed for different reasons. They can be caused by missing processes or incorrect rate constants in the calculations of the production or destruction rates (Sect. 4.2). It is also possible that measured concentrations that are used for the calculation contain unknown errors. The technically difficult radical measurements have a large potential for artifacts (Hofzumahaus and Heard, 2016). Precautions were taken to minimize measurement interferences for OH and HO$_2$ in this campaign.
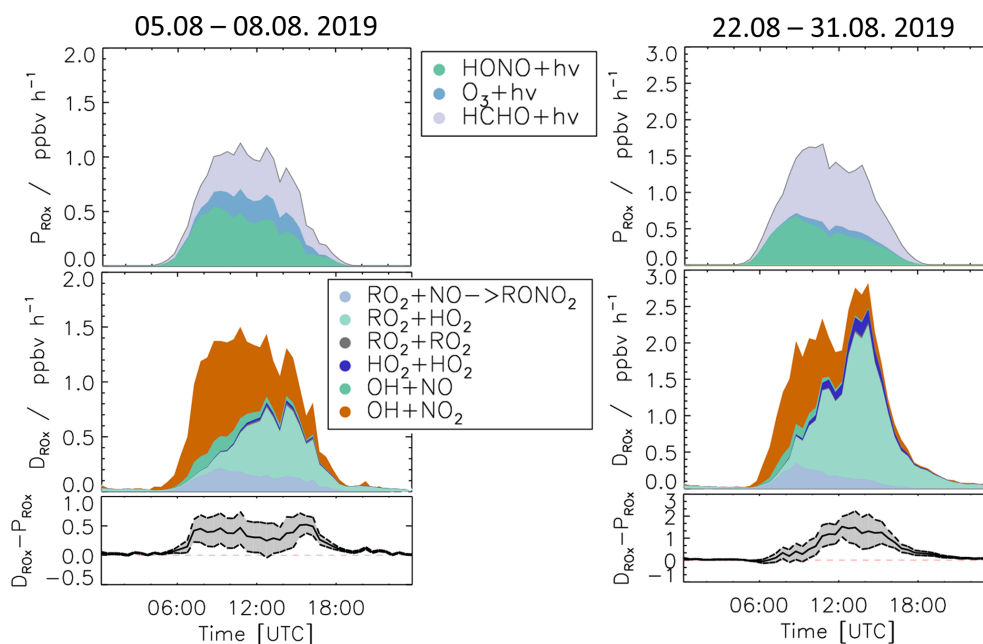
Figure 11. Production and destruction rates of RO$_X$ for the periods of the case studies (Case 1 and Case 2). In addition, the differences between the destruction and production rates are shown. Grey areas indicate the 1σ uncertainty derived from experimental errors of the measured quantities (Table 2) and of the reaction rate constants (Table 1). The reactions that have insignificant contributions to the production or destruction rates are not shown.

- The measurements of OH by the LIF instrument were interference-corrected using chemical modulation and agreed with simultaneous OH measurements by the DOAS instrument within the experimental uncertainties. The measured OH reactivity quantifies the total chemical loss rate of OH caused by atmospheric reactants and has a total accuracy of 10 %. Thus, the destruction rate of OH, which is the product of the concentration and reactivity of OH, is known within 20 % and is unlikely to be biased by unknown OH interferences or unknown atmospheric reactants.

- The O$_x$ production rate calculated from the reaction of peroxy radicals with NO agrees with the measured increase in O$_x$ concentrations within ± 1 ppbv h^{-1} for most conditions (Sect. 3.1). As more than 70 % of the OH production is due to the reaction of HO$_2$ with NO (Reaction R10), a bias of more than 1 ppbv h^{-1} due to an HO$_2$ measurement error that is unaccounted for seems unlikely.

- The analysis of the chemical budget of OH in previous chamber experiments performed at various chemical conditions showed no evidence for a missing OH source originating from chamber wall effects (Kaminski et al., 2017; Fuchs et al., 2018; Novelli et al., 2018; Rolletter et al., 2019; Rolletter et al., 2020).

Thus, there is no evidence for instrumental errors that are not included in the estimated errors of the calculated turnover

rates. The observed imbalances in the OH budget of up to 3 ppbv h^{-1} are therefore most likely due to a missing OH source.

The missing OH production is correlated with the imbalance in the HO$_2$ budget, for which the production rate is larger than the loss rate at low NO mixing ratios (Fig. 12). This is most clearly seen in the period of Case 1, when the discrepancy reaches (2.0 ± 1) ppbv h^{-1} (Fig. 10). The production rate of HO$_2$ is nearly equal to the RO$_2$ loss rate ($P_{HO_2} \approx D_{RO_2}$) because both are controlled by the reaction of RO$_2$ with NO (Reaction R9). Furthermore, the RO$_2$ loss rate is well balanced by the RO$_2$ production rate within the experimental uncertainty of ± 1 ppbv h^{-1} (Figs. 8 and 10). Thus, there is no hint that the calculated turnover rate of the RO$_2$+NO reaction had a bias higher than 1 ppbv h^{-1}. In addition, turnover rates of the reactions of HO$_2$ and RO$_2$ with NO, producing ozone, are consistent with the observed O$_x$ increase in the chamber (Sect. 3.1). This suggests that these rates are correct in the chemical budget analysis. For the above reasons, the discrepancy between HO$_2$ production and destruction rates is most likely due to a missing HO$_2$ loss process and not measurement errors of HO$_2$, RO$_2$, or NO.

RO$_X$ destruction rates are generally higher than the production rates, but differences are on average lower than 0.5 ppbv h^{-1} (Fig. 9). In the periods of Case 1 and Case 2, the corresponding discrepancies reach 0.5 and 1.4 ppbv h^{-1}, respectively (Fig. 10). If these discrepancies were due to a missing primary OH source, they could also explain a small
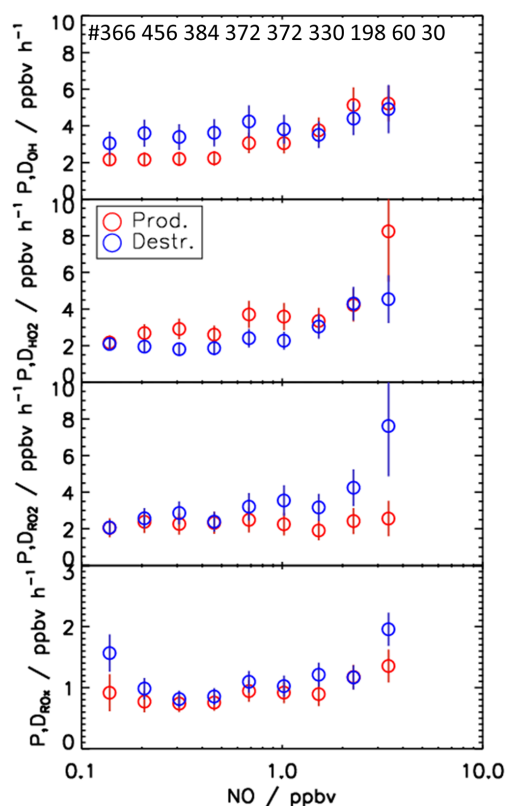
Figure 12. NO dependence of median production and destruction rates of OH, HO$_2$, RO$_2$, and RO$_X$ radicals. Median values include all data from the spring and summer periods of the JULIAC campaign (NO intervals: ln(NO) = 0.4 ppbv). Vertical bars represent the 1σ uncertainty from experimental errors of the measured quantities (Table 2) and of the reaction rate constants (Table 1). The number of data points in each NO bin is represented on the top panel.

part (17 %) of the imbalance in the chemical OH budget in Case 1 and the complete imbalance in the OH budget in Case 2.

It is difficult to identify the exact cause of the differences in OH and HO$_2$ budgets observed for Case 1 and 2 with only the available data. Case 2 was characterized by high temperature with increased BVOC emissions and high levels of HCHO (Table S3). No clear correlation was found between the ratio of the production and destruction rates of the radicals and the concentration of chemical species such as NO, NO$_2$, O$_3$, and HCHO. A weak correlation was observed with temperature with an improved balance in the budgets the higher the temperature was. This could indicate that the processes that are unaccounted for become less competitive for high radical turnover rates with chemical conditions being dominated by organic compounds from biogenic emissions.

In conclusion, the radical budget analysis suggests the presence of a missing OH source and a missing HO$_2$ loss process with a similar turnover rate at NO mixing ratios below 1 ppbv for typical temperatures in summer. The opposing

imbalances in the OH and HO$_2$ budgets could be due to an unknown mechanism that converts HO$_2$ to OH, or they could indicate a missing primary OH source and a similar fast, but independent, termination reaction removing HO$_2$. The remaining imbalance in the RO$_X$ budget would be consistent with a primary OH source that is unaccounted for. This fits the observations best in Case 2, which is characterized by high temperatures and VOC emissions.

For NO mixing ratios that are higher than 1 ppbv, production and destruction rates of OH and HO$_2$ radicals are generally balanced (Fig. 12). An exception is observed for HO$_2$ for the highest NO mixing ratios of 3.5 ppbv, for which the production rate is 3.5 ppbv h^{-1} higher than the loss rate.

For RO$_2$, the radical budget is not closed, but the loss rate increases with NO in contrast to the production rate. The difference reaches a value of 5 ppbv h^{-1} at 3.5 ppbv NO. In the same range of NO mixing ratios, the odd oxygen production rate (P_{O_x}) calculated by peroxy radicals (Eq. 14) overestimates the observed increase in the O$_x$ mixing ratio by about 3 ppbv h^{-1}. This difference points to a systematic error in the peroxy radical measurements, explaining a considerable part of the imbalance in the RO$_2$ budget. A reduction of the RO$_2$ concentration by 3×10^7 cm^{-3} would reduce the HO$_2$ production rate by 3 ppbv h^{-1} and resolve the discrepancy in the odd oxygen production calculations for the highest NO mixing ratio. The presumed bias in the RO$_2$ measurement may be caused by an incorrect background subtraction that becomes most relevant at high NO concentrations (Sect. 3.1). However, even after correction of this bias a discrepancy in the RO$_2$ budget would remain, requiring an additional RO$_2$ source of approximately 2 ppbv h^{-1} to be balanced.

Further information on the nature of the missing RO$_2$ source can be obtained from the chemical budget of RO$_X$, for which the production rate is 0.5 ppbv h^{-1} smaller than the loss rate at 3.5 ppbv NO (Fig. 12). This discrepancy cannot be explained by the instrumental uncertainties in HO$_2$ and RO$_2$ measurements because the RO$_X$ budget at high NO in the morning was dominated by OH reactions with NO$_2$ and (Fig. 9). Thus, the imbalance in the RO$_X$ budget at high NO indicates a missing primary radical source, which on a single day (29 April) even reached 3 ppbv h^{-1} (Fig. 6). As the OH budget is balanced most of the time and the corresponding HO$_2$ budget does not require an additional HO$_2$ source, a missing primary RO$_2$ source is a likely explanation for the discrepancy in the RO$_X$ budget. This would also explain part of the imbalance in the RO$_2$ budget at high NO concentrations.

4.2 Potentially missing chemical processes

The above discussion shows that imbalances between calculated production and destruction rates are highly variable over time and change with chemical conditions. As main general features in spring and summer, the radical budget analysis indicates OH production processes that are unac-

counted for with a typical strength of 1.5–3 ppbv h^{-1} at low NO concentrations, which coincides with a missing HO$_2$ sink of 1–2 ppbv h^{-1}. At high NO mixing ratios (> 1 ppbv), the radical budgets for OH and HO$_2$ radicals are relatively well balanced, but RO$_2$ production processes of about 2 ppbv h^{-1} appear to be missing in the RO$_2$ radical budget. In the following, potential reasons for the observed discrepancies in the radical budgets are discussed.

4.2.1 Differences in the chemical behavior of specific RO$_2$ radicals

As no speciated RO$_2$ radicals were detected but the sum of all RO$_2$ species, effective rate coefficients for the reaction of all RO$_2$ species with NO (Reactions R9, R14), RO$_2$ (Reaction R15), and HO$_2$ (Reaction R16) are used from the structure–activity relationship (SAR) by Jenkin et al. (2019) for the calculations of turnover rates. Potential systematic errors due to this simplification for reactions of RO$_2$ with RO$_2$ and HO$_2$ are expected to be negligible due to their small contributions to the total turnover rates.

In contrast, the reaction of RO$_2$ with NO plays an important role in the chemical budgets of HO$_2$ and RO$_2$. The reaction has one channel that converts RO$_2$ to HO$_2$ (Reaction R9) and one radical termination channel that produces organic nitrates (RONO$_2$) (Reaction R14). The unknown speciation of RO$_2$ causes uncertainty with respect to the total rate constant of the RO$_2$+ NO reaction ($k_9 + k_{14}$). An effective value of 9×10^{-12} cm^3 s^{-1} was taken from Jenkin et al. (2019). A high limit for the total rate coefficient of RO$_2$+ NO (for example, 1.1×10^{-11} cm^3 s^{-1} at 298 K for c-C$_5$H$_9$O$_2$) would slightly increase the imbalances between production and destruction rates for HO$_2$ and RO$_2$ radicals by 13 % for both spring and summer. A lower limit would be the rate constant of the reaction of methyl peroxy radicals (CH$_3$O$_2$) with NO having a value of 7.7×10^{-12} cm^3 s^{-1} (298 K). Applying this number in the calculations for HO$_2$ production and RO$_2$ destruction rates (Fig. S6) for the period when observed discrepancies in the HO$_2$ budget were highest (Case 1) further improves the already well-balanced budget of RO$_2$ radicals. This also reduces the imbalance between HO$_2$ destruction and destruction rates, but the effect is rather small (approximately 10 %) and not sufficient to explain the total difference. For the other periods such as the spring period and the period of Case 2, a reduced reaction rate would worsen the observed imbalances.

An additional uncertainty in the HO$_2$ production rate comes from the assumed yield of organic nitrates in the reaction of RO$_2$ with NO. Typical organic nitrate yields range from 5 % to 20 % (Jenkin et al., 2019). The low-limit value is applied in the calculations above. Using a value of 20 % decreases the discrepancy between HO$_2$ production and destruction rates from 2.0 to 1.5 ppbv h^{-1} for the period of Case 1.

It is worth noting that the organic nitrate yield is generally higher for larger hydrocarbons, but the rate constant for the RO$_2$+ NO reaction is also often higher so that there are compensating effects in the production efficiency of HO$_2$. In addition, it is expected that only a fraction of RO$_2$ radicals produced from large hydrocarbons due to the major composition of RO$_2$ would be methyl peroxy radicals.

For the above reasons, the unknown speciation of RO$_2$ is unlikely to be the reason for the observed imbalances in the HO$_2$ budget that are most prominent in the period of Case 1.

4.2.2 Missing primary radical sources

Primary RO$_X$ radical production that may not be appropriately accounted for in the calculations could be OH, HO$_2$, and RO$_2$ production from the ozonolysis of alkenes. Only a few alkene compounds were measured in the JULIAC campaign. The contribution from the ozonolysis of these alkenes to the radical production was very small with values in the range of 0.005 to 0.03 ppbv h^{-1} (Sect. 3.5). The ozonolysis of small alkenes such as propene and cis-2-butene that were not measured but are often abundant, for example, in forested areas (Goldstein et al., 1996; Rhew et al., 2017) may have significantly contributed to the radical production.

The potential impact of unmeasured alkenes on the primary radical production is tested by assuming that the OH reactivity that cannot be explained by measured OH reactants (on average, 2.5 s^{-1}) originates from 1.5 ppbv propene and 1.0 ppbv cis-2-butene. The radical production by ozonolysis of the additional propene and cis-2-butene increases the production from ozonolysis of measured species by more than an order of magnitude in both the spring and summer periods of the JULIAC campaign (Fig. S7). The discrepancies between the total RO$_X$ production and destruction rates are significantly decreased for the period of 2 Case by approximately 0.2 ppbv h^{-1}. However, the additional OH production is by far insufficient to explain the missing OH source that was generally found during the JULIAC campaign. In addition, the corresponding OH and O$_3$ reactivity from the additional alkene compounds is about a factor of 6 larger than of alkenes (e.g., ethene, propene, $trans$-2-butene, cis-2-pentene) that were measured in ambient air next to the SAPHIR chamber in the HOxComp campaign in July 2005 (Elshorbany et al., 2012; Kanaya et al., 2012).

The photolysis of oxygenated organic compounds is another source for radicals that could be underestimated in the calculations. Only the photolysis of HCHO is included in the production rate of HO$_2$ and RO$_X$ at all times of the campaign. In addition, acetaldehyde (CH$_3$CHO), methyl vinyl ketone (MVK), methacrolein (MACR), and methylglyoxal were measured during part of the campaign and were not included in the analysis in Sect. 3. Calculations show that the radical production rate from their photolysis was less than 0.1 ppbv h^{-1}. Thus, photolysis of unmeasured OVOCs was very likely unimportant in the present study. This is con-

sistent with similar small contributions from photolysis of OVOCs other than HCHO found in the HOxComp campaign (Kanaya et al., 2012). In addition, during the HOxComp campaign the modeled OH reactivity could be matched with the measured reactivity by including either additional primary emissions (Kanaya et al., 2012) or model-produced oxygenated secondary products (Elshorbany et al., 2012). Neither of the additional species contributed enough to close the radical budgets. If it is assumed that the missing OH reactivity (2.5 s^{-1}) is all due to glyoxal (9 ppb), additional OH production of 0.3 ppb h^{-1} could be expected. This would still not be enough to close the radical budget, suggesting that unmeasured OVOCs do not play a large role.

The photolysis of ClNO$_2$ constitutes a primary radical source (Reactions R20, R22) that can be found in coastal environments (e.g., Osthoff et al., 2008) and mid-continental regions (e.g., Thornton et al., 2010). The availability of ClNO$_2$ data during the summer period allowed assessing the potential impact of its photolysis on the RO$_2$ radical production (Eq. 9). Due to the low mixing ratio of ClNO$_2$ of less than 0.4 ppbv (Tan et al., 2022), the RO$_2$ production from Cl oxidation processes was insignificant (<0.1 ppbv h^{-1}) and cannot explain the observed discrepancies in the primary production and destruction rates of radicals in the summer period and in the case studies. The instrument detecting ClNO$_2$ was not available in the spring period of the campaign. Therefore, the extent to which ClNO$_2$ photolysis contributed in spring, for example to the large missing RO$_x$ source (up to 3 ppbv h^{-1}) on 29 April, remains unknown.

4.2.3 Missing radical termination reactions

Heterogeneous uptake of HO$_2$ on aerosol is a potential termination reaction that is not included in the HO$_2$ and RO$_X$ destruction rates above. However, the impact of including the heterogeneous HO$_2$ loss on an aerosol surface (Reaction 8) on the total loss rate is insignificant (less than 1 %), even if a high effective uptake coefficient of 0.2 is assumed (Fig. S7).

As HO$_2$ uptake is a radical termination process, its relative contribution to the total RO$_X$ loss rate can be higher compared to the relative contribution to the total HO$_2$ loss rate. However, the only notable influence would be for the period of Case 2 (8 % of total RO$_X$ loss rate), when aerosol surface area concentration was high with values of up to 3.0×10^2 μm^2 cm^{-3}.

The estimate for the heterogeneous HO$_2$ loss rate has high uncertainty because the uptake coefficient highly depends on the aerosol properties that were not fully characterized in this campaign. Previous laboratory investigations showed large variability for the uptake coefficient with values ranging from 0.08 to 0.6 depending on the aerosol chemical composition and the physical state (George et al., 2007; Taketani et al., 2008, 2009; George et al., 2013; Lakey et al., 2015; Song et al., 2020; Tan et al., 2020). Even the largest reported HO$_2$ uptake coefficients cannot explain the observed differences

in the chemical budget of HO$_2$ radicals. Therefore, heterogeneous HO$_2$ reactions can be ruled out as an explanation for the unexplained HO$_2$ loss rate.

4.2.4 Missing radical interconversion reactions

In the last decade, it has been discovered that unimolecular reactions of RO$_2$ can significantly increase atmospheric OH concentrations in low-NO environments where they can compete with the reaction of RO$_2$ with NO. The most important, atmospherically relevant example is the production of OH from the isomerization of isoprene–RO$_2$ radicals (Peeters et al., 2009; da Silva et al., 2010; Peeters and Müller, 2010; Crounse et al., 2011; Fuchs et al., 2013; Peeters et al., 2014; Teng et al., 2017; Novelli et al., 2020). The SAPHIR chamber is surrounded by a deciduous forest that emits isoprene, especially in summer. Compared to previous campaigns on the campus wherein up to several parts per billion by volume of isoprene were measured (Komenda et al., 2003; Spirig et al., 2005; Kanaya et al., 2012), concentrations were relatively low during the JULIAC campaign (<0.4 ppbv on average).

The effect of the conversion of RO$_2$ to OH by the isomerization of isoprene–RO$_2$ (Eq. 4) is tested in the analysis of the OH and RO$_2$ budgets. In the afternoon of days in the spring period and the period of Case 2, the total OH production increases only 1 % due to the low isoprene mixing ratios (<0.2 ppbv) and the competition of unimolecular reactions with bimolecular reactions of RO$_2$ with NO. Even in the summer period, when isoprene mixing ratios were up to 0.8 ppbv, the contribution of isomerization reactions from isoprene–RO$_2$ radicals to the total turnover rate of RO$_2$ is still small with values of less than 4 %. This implies that unimolecular decomposition reactions of isoprene–RO$_2$ radicals made a minor contribution to the RO$_2$ destruction and OH production rates.

Another known isomerization process that produces OH applies to RO$_2$ formed by OH oxidation of methacrolein (MACR) (Crounse et al., 2012; Fuchs et al., 2014), which is an oxidation product of isoprene. MACR mixing ratios were up to 0.5 ppbv in the JULIAC campaign. Because the rate constant for the OH reaction of MACR is smaller than for isoprene, OH regeneration from MACR-RO$_2$ radicals is even less important than from isoprene–RO$_2$.

For acyl and carbonyl peroxy radicals it was shown that the reaction of RO$_2$ with HO$_2$, which mainly forms hydroperoxides (ROOHs) (Reaction R16), can produce OH with yields up to 80 % (Hasson et al., 2004; Dillon and Crowley, 2008; Groß et al., 2014; Praske et al., 2015; Winiberg et al., 2016; Fuchs et al., 2018; Jenkin et al., 2019). It is also noteworthy that the rate constant for the reaction of HO$_2$ with this class of RO$_2$ species is almost a factor of 2 higher than for other RO$_2$ species (Jenkin et al., 2019). However, even if it is assumed that all the measured RO$_2$ constitutes acyl and carbonyl peroxy radicals, the formation of OH from their reaction with

NO could only explain up to 0.5 ppbv h^{-1} of the imbalances in both OH and HO$_2$ budgets.

Studies in the remote marine boundary layer show that HO$_2$ to OH conversion mediated by halogen oxides (XO, X = Cl, Br, I) (e.g., Bloss et al., 2005; Sommariva et al., 2006; Kanaya et al., 2007; Stone et al., 2018; Fan and Li, 2022) can significantly contribute to the interconversion of radicals and destroy ozone.

$$HO_2 + XO \rightarrow HOX + O_2 \tag{R23}$$
$$HOX + h\nu \rightarrow OH + X \tag{R24}$$
$$XO + NO \rightarrow NO_2 + X \tag{R25}$$
$$X + O_3 \rightarrow XO \tag{R26}$$

This conversion mechanism would only be effective at low NO, when the consumption of XO by NO (Reaction R25) is comparatively slow and when X is not depleted by other reactions as in the case of Cl by reactions with VOCs (Reaction R22).

For BrO, the rate constants for Reactions (R23) and (R25) are about the same (2.1×10^{-11} cm^{-3} s^{-1} at 298 K; Burkholder et al., 2019). Thus, the reaction of BrO with HO$_2$ would only be dominant if the NO concentration were smaller than the concentration of HO$_2$, i.e., less than 10 pptv in this campaign. For IO, the situation is similar and NO mixing ratios would need to be less than 40 pptv. Such low NO mixing ratios were not observed during daytime and rule out significant halogen-oxide-mediated HO$_2$ to OH conversion. The required XO concentrations to achieve an HO$_2$ loss rate of 1 ppbv h^{-1} at an HO$_2$ concentration of 2×10^8 cm^3 would be 66 pptv of BrO or 16 pptv of IO, which exceeds the abundances reported for marine environments, where halogen sources are known to exist, by more than an order of magnitude. For these reasons, halogen oxide chemistry cannot explain the missing HO$_2$ sink and missing OH source in this study.

4.3 Comparison with results from other field campaigns

Although the chemical and physical conditions were partly influenced by the chamber properties (Sect. 2.1), the radical concentrations observed during spring and summer were within the range of values that have been observed in other field studies in summertime in urban and suburban areas (Tan et al., 2001; Ren et al., 2003; Kanaya et al., 2007; Mao et al., 2010; Lu et al., 2013; Brune et al., 2016; Tan et al., 2017; Whalley et al., 2018; Tan et al., 2019). The impact of the decreased solar radiation by the chamber transmission on the radical production was compensated for by the radical production from the photolysis of HONO and HCHO emitted from the chamber film.

This effect is also shown in the relationship between the OH concentration and the photolysis frequencies of ozone, j_{O^1D} (Sect. 3.4). The slope (8.0×10^{11} cm^{-3} s^{-1}) of the correlation for the data from the JULIAC campaign is much higher than obtained for data in other field campaigns in similar environments (Ehhalt and Rohrer, 2000; Handisides et al., 2003; Holland et al., 2003; Tan et al., 2017) due to the high OH production by the photolysis of chamber-produced HONO (Reaction R1). This is further confirmed by the similarity in OH and HO$_2$ radical concentrations between this campaign and what was observed in the HOxComp campaign when measurements were performed in front of the SAPHIR chamber for 3 d in July 2005 (Elshorbany et al., 2012).

In contrast, daytime OH concentrations observed during winter and autumn in the JULIAC campaign were lower than OH concentrations observed in previous wintertime field campaigns (Heard et al., 2004; Ren et al., 2006; Kanaya et al., 2007; Tan et al., 2018; Ma et al., 2019). This is due to the lower photolysis frequencies in the chamber compared to outside, which is not compensated for by chamber-produced HONO in wintertime because the emission strength is low at low temperature and low solar radiation.

The very low nighttime OH concentration in all seasons of the JULIAC campaign (Sect. 3.4) is consistent with observations in previous field campaigns in rural areas in Germany (Ehhalt and Rohrer, 2000; Handisides et al., 2003; Holland et al., 2003), in which nighttime OH concentrations were less than 1×10^5 cm^{-3}. However, in several other field studies performed in urban areas, nighttime OH concentrations were in the range of 0.2 to 3×10^6 cm^{-3}, for example in China (Lu et al., 2014; Rohrer et al., 2014; Tan et al., 2017, 2018; Ma et al., 2019; Tan et al., 2019; Wang et al., 2019; Whalley et al., 2021), in the US (Martinez et al., 2003; Brune et al., 2016; Griffith et al., 2016), and in the UK (Ren et al., 2003; Vaughan et al., 2012). In these studies, the high nighttime OH concentrations could not be explained by model predictions and raised questions about the presence of potential interference in nighttime OH signals measured by LIF instruments (Mao et al., 2012; Lu et al., 2014; Novelli et al., 2014).

Similar studies investigating the chemical budgets of OH, HO$_2$, RO$_2$, and RO$_X$ radicals like in this study were performed for data from field campaigns in a suburban area in the Pearl River Delta (PRD), China, in autumn 2014 (Tan et al., 2019), and in central Beijing, China (Whalley et al., 2021), in summer 2017.

Tan et al. (2019) observed median values of turnover rates of OH, HO$_2$, and RO$_2$ radicals ranging from 10 to 15 ppbv h^{-1}, while rates for RO$_X$ initiation and termination were on the order of 3 to 4 ppbv h^{-1} during daytime for chemical conditions affected by anthropogenic emissions. From the comparison between the radical production and destruction rates, a missing OH source and a missing RO$_2$ sink with a similar rate up to 7 ppbv h^{-1} (45 % of the total OH turnover) were found at low NO mixing ratios below 1 ppbv, while HO$_2$ production and destruction rates were balanced. The authors suggested that an additional chemical mechanism is required that efficiently converts RO$_2$ to OH without the involvement of NO. One possibility proposed by Tan et

al. (2019) is that HO_X radicals are formed from the auto-oxidation of specific RO_2 species which include multifunctional groups such as -OH, -OOH, or -CHO groups.

The analysis of the chemical budget of OH radicals in the JULIAC campaign shows that an OH source that is unaccounted for with a rate ranging between 2 and 3 ppbv h^{-1} (about 50 % of the total OH destruction rate) is required at low NO mixing ratios to balance OH production and destruction rates. This rate is smaller than the rate determined in Tan et al. (2019). However, considering that the OH radical turnover rates in the JULIAC campaign were about half compared to values in the campaign in the PRD area, the relative importance of the unaccounted for OH source was comparable in both campaigns. However, the mechanism suggested by Tan et al. (2019) is likely not the only explanation for discrepancies in the radical budgets observed in this study. In the JULIAC campaign, to balance the budget of RO_2 radicals requires an additional radical source rather than additional loss processes, particularly at high NO mixing ratios above 1 ppbv, and the missing OH sources likely originate from an HO_2 to OH conversion process and/or a missing primary OH source.

Whalley et al. (2021) also investigated the chemical budgets for radicals over a wide range of NO mixing ratios (0.1 to 104 ppbv) from measurements performed in central Beijing, China. Compared to the results in Tan et al. (2019) and results in this study, the rates of RO_X initiation and termination reactions were 2 to 4 times higher. Also, the rates of radical propagation reactions for OH, HO_2, and RO_2 radicals were 5 to 10 times higher due to fast inter-radical conversion reactions at conditions with high concentrations of NO. Similar to the results in this study, an OH source with a high rate of up to 15 ppbv h^{-1} (50 % of the total OH destruction) was required to balance OH production and destruction rates for low NO mixing ratios. This unaccounted for OH source is more than 3 times higher than that determined in the JULIAC campaign and in the campaign in China reported by Tan et al. (2019). The HO_2 production rate observed in Beijing largely exceeded the destruction rate by 3 to 5 times for low NO mixing ratios. In contrast, production and destruction of RO_2 and RO_X radicals were well balanced. On the other hand, for results in conditions of low NO concentrations, production and destruction of OH radicals were balanced at high NO mixing ratios, while very high imbalances of up to 50 ppbv h^{-1} were observed for HO_2 and RO_2 radicals. Whalley et al. (2021) showed that reducing the rate constant of the reaction between RO_2 and NO by a factor of 10 could close the gaps between production and destruction rates. The authors suggested that the presence of a significant fraction of RO_2 radicals from the oxidation of large and multifunctional VOCs such as monoterpenes and long-chain alkanes could explain observations. These radicals can undergo multiple RO_2 to RO_2 conversion reactions by unimolecular isomerization of alkoxy radicals (RO), which are formed from the reaction of RO_2 with NO so that no HO_2

is produced. Such an RO_2 radical reaction chain would be equivalent to an increased chemical lifetime of RO_2 radicals if RO_2 species cannot be distinguished by instruments like in the sum measurements performed by RO_X–LIF instruments. Whalley et al. (2021) showed that RO_2 production by this mechanism would largely reconcile discrepancies between modeled and measured RO_2 concentrations (the model–measurement ratio decreases from 6.2 to 1.8) if the OH reactivity that could not be accounted for by measured OH reactants is attributed to α-pinene.

Applying a reduced rate constant for RO_2 to HO_2 propagation reactions as suggested in Whalley et al. (2021) in the calculations in this study could help explain the observed discrepancies between HO_2 and RO_2 production and destruction rates. The largest effect is expected when high NO mixing ratios up to 10 ppbv like on 29 April are experienced. In this case, a large reduction of the rate constant by a factor of 2 for all measured RO_2 would be required to close the observed gaps between production and destruction rates. Reduced reaction rate constants of the $RO_2 + NO$ reaction could be expected for RO_2 from large VOCs. However, the fraction of these RO_2 species is expected to be small for conditions of this campaign, even if OH reactivity that is not explained by measured OH reactants is attributed to large VOCs. Therefore, it seems unlikely that the mechanism suggested by Whalley et al. (2021) affects the observed discrepancies in the radical budgets in this study.

It is interesting to point out that similar discrepancies in the OH and HO_2 budgets were observed during the HOxComp campaign in July 2005 (Elshorbany et al., 2012). Although measurements were only done for 3 d and despite the fact that these were 14 years earlier than measurements in this work, the chemical composition was similar with comparable values of NO_x, O_3, isoprene concentrations, and OH reactivity. As observed in this study, a missing OH radical source in the range of 2 to 4 ppbv h^{-1} was needed to close the OH budget for low-NO chemical regimes. The lack of measured RO_2 radicals did not allow performing a measurement-only budget for HO_2 radicals. Nevertheless, model calculations overestimated measured HO_2 radicals after the correction for RO_2 radical interference (Fuchs et al., 2011) by up to 30 % at low NO (Elshorbany et al., 2012; Kanaya et al., 2012). Like in this study, good agreement was found between modeled and measured OH and HO_2 radical concentrations only if an unknown loss process for HO_2 radicals that would recycle OH was introduced.

4.4 Potential role of the missing radical processes in the evaluation of the ozone production rate

The good agreement of the odd oxygen production rates calculated by the two different methods (Sect. 3.1) not only gives high confidence in the measured peroxy radical concentrations but also confirms the current chemical understanding of tropospheric ozone formation from the reaction

of peroxy radicals with NO. Therefore, results demonstrate that accurate predictions of radical concentrations in atmospheric models are crucial to accurately predict the surface ozone level.

However, the significant level of missing radical processes found in this study implies difficulties in the prediction of radical concentrations by models without constraining radicals by their measurements. In low NO mixing ratios, there are two opposing effects of the missing radical processes on the O$_3$ formation. At first, a missing OH source and therefore an underestimation of OH concentrations by the models would lower the loss of NO$_2$ by the reduced reaction rate with OH and essentially produce more O$_3$ by its photolysis. Furthermore, the production of RO$_2$ would be underpredicted due to the lower OH concentrations in the models. At the same time, an unexplained HO$_2$ sink would result in the overprediction of HO$_2$ concentrations and thus O$_3$ production. In high-NO environments, missing RO$_2$ and RO$_X$ production processes would result in an underestimation of the O$_3$ production.

5 Summary and conclusions

Ambient measurements of atmospheric radicals, trace gases, and aerosol properties were performed during the Jülich Atmospheric Chemistry (JULIAC) project campaign using the atmospheric simulation chamber SAPHIR at Forschungszentrum Jülich, Germany. Ambient air was continuously drawn at a high rate into the chamber (1 h residence time) through a 50 m high inlet line for 1 month in each season throughout 2019.

For parts of the campaign, measurements of OH concentrations were achieved by two different methods, laser-induced fluorescence with a chemical modulation system for zeroing (FZJ LIF–CMR) and differential optical absorption spectroscopy (FZJ DOAS). Measurements of both instruments agreed within 11 % (Cho et al., 2021).

The production rate of odd oxygen (O$_x$) was determined by using either measured HO$_2$ and RO$_2$ concentrations or O$_3$ and NO$_2$ concentrations measured in the chamber and in the incoming flow. Results showed excellent agreement between the two different methods, confirming that HO$_2$ and RO$_2$ are responsible for the formation of tropospheric O$_3$ and giving additional confidence to the reliability of peroxy radical concentration measurements performed in the JULIAC campaign.

An analysis of the chemical budgets of OH, HO$_2$, RO$_2$, and RO$_X$ radicals was performed for data obtained in the spring and summer periods of the campaign. On average, daytime radical turnover rates ranged between 3 and 6 ppbv h^{-1} and between 4 and 10 ppbv h^{-1} in spring and summer, respectively, for OH, HO$_2$, and RO$_2$ radicals, while total rates of RO$_X$ initiation and termination reactions were below 2.0 ppbv h^{-1}. For most conditions, radical production

and destruction rates highly depended on the turnover rate of the reaction of peroxy radicals with NO. For the total turnover rate of the sum of all radicals (RO$_X$), the photolysis of HONO and HCHO contributed most to the primary radical production, and the reactions of OH with NO$_2$ and RO$_2$ with HO$_2$ dominated the radical termination processes.

Differences between radical production and destruction rates were often small and below the accuracy of the calculations in the JULIAC campaign in winter and autumn. However, for both spring and summer, an additional OH source is required to explain the observed discrepancy between production and destruction rates. The OH production rate of this source would need be on average 2 and 3 ppbv h^{-1} in the spring and summer period, respectively. This discrepancy is in the same range as observed for measurements at the same location during the HOxComp campaign in July 2005 (Elshorbany et al., 2012).

Discrepancies between production and destruction rates of OH radicals were highest for conditions with low NO mixing ratios in this study. This is similar to findings in other field campaigns in China (Tan et al., 2017, 2019; Whalley et al., 2021). The high reliability of radical data in this study gives further confidence that the discrepancies arise from chemical processes that are unaccounted for rather than from instrumental artifacts.

The highest unaccounted for OH source with a rate of 3.0 ppbv h^{-1} (51 % of the observed total OH destruction rate) is observed in the period from 5 to 8 August (Case 1), when NO mixing ratios were less than 1 ppbv and median maximum temperatures in the chamber were 31 °C. At the same time, an additional HO$_2$ destruction process with a rate of up to 2.0 ppbv h^{-1} is required to balance the HO$_2$ production rate, while production and destruction rates for RO$_2$ radicals are well balanced. The opposing imbalances in the OH and HO$_2$ budgets could be due to an unknown mechanism that converts HO$_2$ to OH, or this could indicate a missing primary OH source and a similar fast, but independent, termination reaction removing HO$_2$. If an unknown HO$_2$ to OH conversion mechanism played a major role, it would not explain the complete rate of the missing OH source. Since the missing OH source is slightly larger than the rate of the missing HO$_2$ sink, part of the missing OH source could have originated from a missing primary OH production process because a small difference between the total RO$_X$ production and destruction rates is also observed. The missing RO$_X$ source was up to 0.5 ppbv h^{-1} for Case 1 but was even higher with a rate of 1.4 ppbv h^{-1} in the summer when temperature was highest (Case 2). Since the calculated reaction rates of the HO$_2$ and RO$_2$ radicals with NO were able to reproduce the observed O$_x$ production within 1 ppbv h^{-1}, the unknown missing processes do not seem to have a direct impact on net ozone production.

For NO mixing ratios in the range of 1 to 3 ppbv, production and destruction rates for OH and HO$_2$ radicals were balanced, while additional sources of RO$_2$ and RO$_X$ hav-

ing average rates of 1.6 and 0.4 ppbv h^{-1}, respectively, were required to balance their production and destruction rates. Therefore, part of the missing RO$_2$ source can be explained by a primary radical source, but the remaining RO$_2$ source is still unresolved.

For high NO mixing ratios above 3 ppbv (4 to 5 ppbv h^{-1}), large discrepancies between production and destruction rates of HO$_2$ and RO$_2$ radicals were found, but the calculations for these conditions have a higher uncertainty due to low HO$_2$ and RO$_2$ concentrations close to background signals. Whereas the imbalance in the budget for HO$_2$ radicals is due to a loss process that is unaccounted for, an additional RO$_2$ production process is required to close the chemical budget for RO$_2$ radicals. For the same conditions, a primary RO$_X$ source with a rate of 0.5 ppbv h^{-1} was needed to balance the RO$_X$ destruction rate. Therefore, the missing primary RO$_X$ source is likely a primary RO$_2$ source that is unaccounted for.

Production of radicals from the oxidation of organic compounds by chlorine could have been one additional source. Unfortunately, the potential impact of chlorine chemistry could not be examined in the spring periods, when these conditions were experienced, because ClNO$_2$ measurements were not available. During times when ClNO$_2$ concentrations were measured, chlorine chemistry initiated by the photolysis of ClNO$_2$ did not significantly contribute to the radical production.

For chemical conditions when the contribution of the reaction of HO$_2$ with NO to the OH production was reduced, i.e., at lower NO levels, other radical formation pathways such as isomerization reactions of RO$_2$ radicals, OH formation from ozonolysis of alkenes, or photolysis of multifunctional organic compounds could gain importance and need to be properly accounted for. These processes remain relatively poorly constrained due to the lack of direct measurements of, e.g., multifunctional organic compounds.

Although the exact mechanism for the missing production or destruction processes for OH, HO$_2$, and RO$_2$ radicals could not be determined from measurements in this campaign, knowing the magnitudes of the missing radical processes gives indicative information about the disagreements of model simulations and observations for radicals and secondary air pollutants.

More investigations of the chemical budgets of radicals, for example in environments with high NO mixing ratios, including the determination of the impact of chlorine chemistry and with a detailed characterization of the chemical composition of air masses with respect to the presence of complex organic compounds, would be beneficial for the understanding of radical chemistry as well as the formation of secondary air pollution such as ozone.

Author contributions. AH designed the JULIAC campaign and organized it together with HF and FH. CC performed the measurements of radicals, analyzed the data, and wrote the paper together with AN and HF. All co-authors contributed with data and helped the writing through intensive discussions of the paper.

References

Atkinson, R., Baulch, D. L., Cox, R. A., Crowley, J. N., Hampson, R. F., Hynes, R. G., Jenkin, M. E., Rossi, M. J., and Troe, J.: Evaluated kinetic and photochemical data for atmospheric chemistry: Volume I – gas phase reactions of O$_x$, HO$_x$, NO$_x$ and SO$_x$ species, Atmos. Chem. Phys., 4, 1461–1738, https://doi.org/10.5194/acp-4-1461-2004, 2004.

Atkinson, R., Baulch, D. L., Cox, R. A., Crowley, J. N., Hampson, R. F., Hynes, R. G., Jenkin, M. E., Rossi, M. J., Troe, J., and Subcommittee, I.: Evaluated kinetic and photochemical data for atmospheric chemistry: Volume II – gas phase reactions of organic species, Atmos. Chem. Phys., 6, 3625–4055, https://doi.org/10.5194/acp-6-3625-2006, 2006.

Bloss, W. J., Lee, J. D., Johnson, G. P., Sommariva, R., Heard, D. E., Saiz-Lopez, A., Plane, J. M. C., McFiggans, G., Coe, H., Flynn, M., Williams, P., Rickard, A. R., and Fleming, Z. L.: Impact of halogen monoxide chemistry upon boundary layer OH and HO$_2$ concentrations at a coastal site, Geophys. Res. Lett., 32, 1–4, https://doi.org/10.1029/2004GL022084, 2005.

BMEL (Federal Ministry of Food and Agriculture): Ergebnisse der Waldzustandserhebung 2020, Bonn, Germany, https://www.bmel.de/ (last access: January 2023), 2021.

Bohn, B., Rohrer, F., Brauers, T., and Wahner, A.: Actinometric measurements of NO$_2$ photolysis frequencies in the atmosphere simulation chamber SAPHIR, Atmos. Chem. Phys., 5, 493–503, https://doi.org/10.5194/acp-5-493-2005, 2005.

Bohn, B. and Zilken, H.: Model-aided radiometric determination of photolysis frequencies in a sunlit atmosphere simulation chamber, Atmos. Chem. Phys., 5, 191–206, https://doi.org/10.5194/acp-5-191-2005, 2005.

Brune, W. H., Baier, B. C., Thomas, J., Ren, X., Cohen, R. C., Pusede, S. E., Browne, E. C., Goldstein, A. H., Gentner, D. R., Keutsch, F. N., Thornton, J. A., Harrold, S., Lopez-Hilfiker, F. D., and Wennberg, P. O.: Ozone production chemistry in the presence of urban plumes, Faraday Discuss., 189, 169–189, https://doi.org/10.1039/C5FD00204D, 2016.

Burkholder, J. B., Sander, S. P., Abbatt, J., Barker, J. R., Cappa, C., Crounse, J. D., Dibble, T. S., Huie, R. E., Kolb, C. E., Kurylo, M. J., Orkin, V. L., Percival, C. J., Wilmouth, D. M., and Wine, P. H.: Chemical Kinetics and Photochemical Data for Use in Atmospheric Studies, Evaluation No. 19, JPL Publication 19-5, Jet Propulsion Laboratory, Pasadena, https://jpldataeval.jpl.nasa.gov/ (last access: January 2023), 2019.

Cazorla, M., Brune, W. H., Ren, X., and Lefer, B.: Direct measurement of ozone production rates in Houston in 2009 and comparison with two estimation methods, Atmos. Chem. Phys., 12, 1203–1212, https://doi.org/10.5194/acp-12-1203-2012, 2012.

Chen, S., Ren, X., Mao, J., Chen, Z., Brune, W. H., Lefer, B., Rappenglück, B., Flynn, J., Olson, J., and Crawford, J. H.: A comparison of chemical mechanisms based on TRAMP-2006 field data, Atmos. Environ., 44, 4116–4125, https://doi.org/10.1016/j.atmosenv.2009.05.027, 2010.

Cho, C., Hofzumahaus, A., Fuchs, H., Dorn, H. P., Glowania, M., Holland, F., Rohrer, F., Vardhan, V., Kiendler-Scharr, A., Wahner, A., and Novelli, A.: Characterization of a chemical modulation reactor (CMR) for the measurement of atmospheric concentrations of hydroxyl radicals with a laser-induced fluorescence instrument, Atmos. Meas. Tech., 14, 1851–1877, https://doi.org/10.5194/amt-14-1851-2021, 2021.

Cox, R. A., Ammann, M., Crowley, J. N., Herrmann, H., Jenkin, M. E., McNeill, V. F., Mellouki, A., Troe, J., and Wallington, T. J.: Evaluated kinetic and photochemical data for atmospheric chemistry: Volume VII – Criegee intermediates, Atmos. Chem. Phys., 20, 13497–13519, https://doi.org/10.5194/acp-20-13497-2020, 2020.

Crounse, J. D., Paulot, F., Kjaergaard, H. G., and Wennberg, P. O.: Peroxy radical isomerization in the oxidation of isoprene, Phys. Chem. Chem. Phys., 13, 13607–13613, https://doi.org/10.1039/C1CP21330J, 2011.

Crounse, J. D., Knap, H. C., Ørnsø, K. B., Jørgensen, S., Paulot, F., Kjaergaard, H. G., and Wennberg, P. O.: Atmospheric Fate of Methacrolein, 1. Peroxy Radical Isomerization Following Addition of OH and O$_2$, J. Phys. Chem. A, 116, 5756–5762, https://doi.org/10.1021/jp211560u, 2012.

da Silva, G., Graham, C., and Wang, Z.-F.: Unimolecular â-hydroxyperoxy radical decomposition with OH recycling in the photochemical oxidation of isoprene, Environ. Sci. Technol., 44, 250–256, https://doi.org/10.1021/es900924d, 2010.

Dillon, T. J. and Crowley, J. N.: Direct detection of OH formation in the reactions of HO$_2$ with CH$_3$C(O)O$_2$ and other substituted peroxy radicals, Atmos. Chem. Phys., 8, 4877–4889, https://doi.org/10.5194/acp-8-4877-2008, 2008.

Dusanter, S., Vimal, D., Stevens, P. S., Volkamer, R., Molina, L. T., Baker, A., Meinardi, S., Blake, D., Sheehy, P., Merten, A., Zhang, R., Zheng, J., Fortner, E. C., Junkermann, W., Dubey, M., Rahn, T., Eichinger, B., Lewandowski, P., Prueger, J., and Holder, H.: Measurements of OH and HO$_2$ concentrations during the MCMA-2006 field campaign – Part 2: Model comparison and radical budget, Atmos. Chem. Phys., 9, 6655–6675, https://doi.org/10.5194/acp-9-6655-2009, 2009.

Ehhalt, D. H. and Rohrer, F.: Dependence of the OH concentration on solar UV, J. Geophys. Res.-Atmos., 105, 3565–3571, https://doi.org/10.1029/1999jd901070, 2000.

Elshorbany, Y. F., Kleffmann, J., Hofzumahaus, A., Kurtenbach, R., Wiesen, P., Brauers, T., Bohn, B., Dorn, H.-P., Fuchs, H., Holland, F., Rohrer, F., Tillmann, R., Wegener, R., Wahner, A., Kanaya, Y., Yoshino, A., Nishida, S., Kajii, Y., Martinez, M., Kubistin, D., Harder, H., Lelieveld, J., Elste, T., Plass-Dülmer, C., Stange, G., Berresheim, H., and Schurath, U.: HO$_x$ budgets during HOxComp: A case study of HO$_x$ chemistry under NO$_x$-limited conditions, J. Geophys. Res.-Atmos., 117, D03307, https://doi.org/10.1029/2011JD017008, 2012.

Fan, S. and Li, Y.: The impacts of marine-emitted halogens on OH radicals in East Asia during summer, Atmos. Chem. Phys., 22, 7331–7351, https://doi.org/10.5194/acp-22-7331-2022, 2022.

Fishman, J. and Carney, T. A.: A one-dimensional photochemical model of the troposphere with planetary boundary-layer parameterization, J. Atmos. Chem., 1, 351–376, https://doi.org/10.1007/BF00053800, 1984.

Fuchs, H., Holland, F., and Hofzumahaus, A.: Measurement of tropospheric RO$_2$ and HO$_2$ radicals by a laser-induced fluorescence instrument, Rev. Sci. Instrum., 79, 084104, https://doi.org/10.1063/1.2968712, 2008.

Fuchs, H., Bohn, B., Hofzumahaus, A., Holland, F., Lu, K. D., Nehr, S., Rohrer, F., and Wahner, A.: Detection of HO$_2$ by laser-induced fluorescence: calibration and interferences from RO$_2$ radicals, Atmos. Meas. Tech., 4, 1209–1225, https://doi.org/10.5194/amt-4-1209-2011, 2011.

Fuchs, H., Dorn, H. P., Bachner, M., Bohn, B., Brauers, T., Gomm, S., Hofzumahaus, A., Holland, F., Nehr, S., Rohrer, F., Tillmann, R., and Wahner, A.: Comparison of OH concentration measurements by DOAS and LIF during SAPHIR chamber experiments at high OH reactivity and low NO concentration, Atmos. Meas. Tech., 5, 1611–1626, https://doi.org/10.5194/amt-5-1611-2012, 2012.

Fuchs, H., Hofzumahaus, A., Rohrer, F., Bohn, B., Brauers, T., Dorn, H. P., Häseler, R., Holland, F., Kaminski, M., Li, X., Lu, K., Nehr, S., Tillmann, R., Wegener, R., and Wahner, A.: Experimental evidence for efficient hydroxyl radical regeneration in isoprene oxidation, Nat. Geosci., 6, 1023–1026, https://doi.org/10.1038/ngeo1964, 2013.

Fuchs, H., Acir, I. H., Bohn, B., Brauers, T., Dorn, H. P., Häseler, R., Hofzumahaus, A., Holland, F., Kaminski, M., Li, X., Lu, K., Lutz, A., Nehr, S., Rohrer, F., Tillmann, R., Wegener, R., and Wahner, A.: OH regeneration from methacrolein oxidation investigated in the atmosphere simulation chamber SAPHIR, Atmos. Chem. Phys., 14, 7895–7908, https://doi.org/10.5194/acp-14-7895-2014, 2014.

Fuchs, H., Novelli, A., Rolletter, M., Hofzumahaus, A., Pfannerstill, E. Y., Kessel, S., Edtbauer, A., Williams, J., Michoud, V., Dusanter, S., Locoge, N., Zannoni, N., Gros, V., Truong, F., Sarda-Esteve, R., Cryer, D. R., Brumby, C. A., Whalley, L. K., Stone, D., Seakins, P. W., Heard, D. E., Schoemaecker, C., Blocquet, M., Coudert, S., Batut, S., Fittschen, C., Thames, A. B., Brune, W. H., Ernest, C., Harder, H., Muller, J. B. A., Elste, T., Kubistin, D., Andres, S., Bohn, B., Hohaus, T., Holland, F., Li, X., Rohrer, F., Kiendler-Scharr, A., Tillmann, R., Wegener, R., Yu, Z., Zou, Q., and Wahner, A.: Comparison of OH reactivity measurements in the atmospheric simulation chamber SAPHIR, Atmos. Meas. Tech., 10, 4023–4053, https://doi.org/10.5194/amt-10-4023-2017, 2017.

Fuchs, H., Albrecht, S., Acir, I., Bohn, B., Breitenlechner, M., Dorn, H. P., Gkatzelis, G. I., Hofzumahaus, A., Holland, F., Kaminski, M., Keutsch, F. N., Novelli, A., Reimer, D., Rohrer, F., Tillmann, R., Vereecken, L., Wegener, R., Zaytsev, A., Kiendler-Scharr, A., and Wahner, A.: Investigation of the oxidation of methyl vinyl ketone (MVK) by OH radicals in the atmospheric simulation chamber SAPHIR, Atmos. Chem. Phys., 18, 8001–8016, https://doi.org/10.5194/acp-18-8001-2018, 2018.

George, I. J., Vlasenko, A., Slowik, J. G., Broekhuizen, K., and Abbatt, J. P. D.: Heterogeneous oxidation of saturated organic aerosols by hydroxyl radicals: uptake kinetics, condensed-phase products, and particle size change, Atmos. Chem. Phys., 7, 4187–4201, https://doi.org/10.5194/acp-7-4187-2007, 2007.

George, I. J., Matthews, P. S. J., Whalley, L. K., Brooks, B., Goddard, A., Baeza-Romero, M. T., and Heard, D. E.: Measurements of uptake coefficients for heterogeneous loss of HO$_2$ onto submicron inorganic salt aerosols, Phys. Chem. Chem. Phys, 15, 12829–12845, https://doi.org/10.1039/C3CP51831K, 2013.

Glowania, M., Rohrer, F., Dorn, H.-P., Hofzumahaus, A., Holland, F., Kiendler-Scharr, A., Wahner, A., and Fuchs, H.: Comparison of formaldehyde measurements by Hantzsch, CRDS and DOAS in the SAPHIR chamber, Atmos. Meas. Tech., 14, 4239–4253, https://doi.org/10.5194/amt-14-4239-2021, 2021.

Goldberg, D. L., Vinciguerra, T. P., Hosley, K. M., Loughner, C. P., Canty, T. P., Salawitch, R. J., and Dickerson, R. R.: Evidence for an increase in the ozone photochemical lifetime in the eastern United States using a regional air quality model, J. Geophys. Res.-Atmos., 120, 12778–12793, https://doi.org/10.1002/2015JD023930, 2015.

Goldstein, A. H. and Galbally, I. E.: Known and Unexplored Organic Constituents in the Earth's Atmosphere, Environ. Sci. Technol., 41, 1514–1521, https://doi.org/10.1021/es072476p, 2007.

Goldstein, A. H., Fan, S. M., Goulden, M. L., Munger, J. W., and Wofsy, S. C.: Emissions of ethene, propene, and 1-butene by a midlatitude forest, J. Geophys. Res.-Atmos., 101, 9149–9157, https://doi.org/10.1029/96JD00334, 1996.

Griffith, S. M., Hansen, R. F., Dusanter, S., Stevens, P. S., Alaghmand, M., Bertman, S. B., Carroll, M. A., Erickson, M., Galloway, M., Grossberg, N., Hottle, J., Hou, J., Jobson, B. T., Kammrath, A., Keutsch, F. N., Lefer, B. L., Mielke, L. H., O'Brien, A., Shepson, P. B., Thurlow, M., Wallace, W., Zhang, N., and Zhou, X. L.: OH and HO$_2$ radical chemistry during PROPHET 2008 and CABINEX 2009 – Part 1: Measurements and model comparison, Atmos. Chem. Phys., 13, 5403–5423, https://doi.org/10.5194/acp-13-5403-2013, 2013.

Griffith, S. M., Hansen, R. F., Dusanter, S., Michoud, V., Gilman, J. B., Kuster, W. C., Veres, P. R., Graus, M., de Gouw, J. A., Roberts, J., Young, C., Washenfelder, R., Brown, S. S., Thalman, R., Waxman, E., Volkamer, R., Tsai, C., Stutz, J., Flynn, J. H., Grossberg, N., Lefer, B., Alvarez, S. L., Rappenglueck, B., Mielke, L. H., Osthoff, H. D., and Stevens, P. S.: Measurements of hydroxyl and hydroperoxy radicals during CalNex-LA: Model comparisons and radical budgets, J. Geophys. Res.-Atmos., 121, 4211–4232, https://doi.org/10.1002/2015jd024358, 2016.

Groß, C. B. M., Dillon, T. J., Schuster, G., Lelieveld, J., and Crowley, J. N.: Direct Kinetic Study of OH and O$_3$ Formation in the Reaction of CH$_3$C(O)O$_2$ with HO$_2$, J. Phys. Chem. A, 118, 974–985, https://doi.org/10.1021/jp412380z, 2014.

Han, S., Bian, H., Feng, Y., Liu, A., Li, X., Zeng, F., and Zhang, X.: Analysis of the Relationship between O$_3$, NO and NO$_2$ in Tianjin, China, Aerosol Air Qual. Res., 11, 128–139, https://doi.org/10.4209/aaqr.2010.07.0055, 2011.

Handisides, G. M., Plass-Dülmer, C., Gilge, S., Bingemer, H., and Berresheim, H.: Hohenpeissenberg Photochemical Experiment (HOPE 2000): Measurements and photostationary state calculations of OH and peroxy radicals, Atmos. Chem. Phys., 3, 1565–1588, https://doi.org/10.5194/acp-3-1565-2003, 2003.

Häseler, R., Brauers, T., Holland, F., and Wahner, A.: Development and application of a new mobile LOPAP instrument for the measurement of HONO altitude profiles in the planetary boundary layer, Atmos. Meas. Tech. Discuss., 2, 2027–2054, https://doi.org/10.5194/amtd-2-2027-2009, 2009.

Hasson, A. S., Tyndall, G. S., and Orlando, J. J.: A Product Yield Study of the Reaction of HO$_2$ Radicals with Ethyl Peroxy (C$_2$H$_5$O$_2$), Acetyl Peroxy (CH$_3$C(O)O$_2$), and Acetonyl Peroxy (CH$_3$C(O)CH$_2$O$_2$) Radicals, J. Phys. Chem. A, 108, 5979–5989, https://doi.org/10.1021/jp048873t, 2004.

Hausmann, M., Brandenburger, U., Brauers, T., and Dorn, H.-P.: Detection of tropospheric OH radicals by long-path differential optical-absorption spectroscopy: Experimental setup, accuracy, and precision, J. Geophys. Res., 102, 16011–16022, https://doi.org/10.1029/97jd00931, 1997.

Heard, D. E., Carpenter, L. J., Creasey, D. J., Hopkins, J. R., Lee, J. D., Lewis, A. C., Pilling, M. J., Seakins, P. W., Carslaw, N., and Emmerson, K. M.: High levels of the hydroxyl radical in the winter urban troposphere, Geophys. Res. Lett., 31, L18112, https://doi.org/10.1029/2004GL020544, 2004.

Hens, K., Novelli, A., Martinez, M., Auld, J., Axinte, R., Bohn, B., Fischer, H., Keronen, P., Kubistin, D., Nölscher, A. C., Oswald, R., Paasonen, P., Petäjä, T., Regelin, E., Sander, R., Sinha, V., Sipilä, M., Taraborrelli, D., Tatum Ernest, C., Williams, J., Lelieveld, J., and Harder, H.: Observation and modelling of HO$_x$ radicals in a boreal forest, Atmos. Chem. Phys., 14, 8723–8747, https://doi.org/10.5194/acp-14-8723-2014, 2014.

Hofzumahaus, A., Rohrer, F., Lu, K., Bohn, B., Brauers, T., Chang, C.-C., Fuchs, H., Holland, F., Kita, K., Kondo, Y., Li, X., Lou, S., Shao, M., Zeng, L., Wahner, A., and Zhang, Y.: Amplified

trace gas removal in the troposphere, Science, 324, 1702–1704, https://doi.org/10.1126/science.1164566, 2009.

Hofzumahaus, A. and Heard, D. H.: Assessment of local HO$_x$ and RO$_x$ measurement techniques: achivements, challenges, and future directions – Outcomes of the 2015 international HO$_x$ workshop, Forschungszentrum Jülich, Jülich, 20–21, https://juser.fz-juelich.de/record/826803 (last access: January 2023), 2016.

Holland, F., Hofzumahaus, A., Schäfer, J., Kraus, A., and Pätz, H.-W.: Measurements of OH and HO$_2$ radical concentrations and photolysis frequencies during BERLIOZ, J. Geophys. Res.-Atmos., 108, 8246, https://doi.org/10.1029/2001jd001393, 2003.

Jenkin, M. E., Valorso, R., Aumont, B., and Rickard, A. R.: Estimation of rate coefficients and branching ratios for reactions of organic peroxy radicals for use in automated mechanism construction, Atmos. Chem. Phys., 19, 7691–7717, https://doi.org/10.5194/acp-19-7691-2019, 2019.

Jordan, A., Haidacher, S., Hanel, G., Hartungen, E., Märk, L., Seehauser, H., Schottkowsky, R., Sulzer, P., and Märk, T. D.: A high resolution and high sensitivity proton-transfer-reaction time-of-flight mass spectrometer (PTR-TOF-MS), Int. J. Mass Spectrom., 286, 122–128, https://doi.org/10.1016/j.ijms.2009.07.005, 2009.

Kaminski, M., Fuchs, H., Acir, I. H., Bohn, B., Brauers, T., Dorn, H. P., Häseler, R., Hofzumahaus, A., Li, X., Lutz, A., Nehr, S., Rohrer, F., Tillmann, R., Vereecken, L., Wegener, R., and Wahner, A.: Investigation of the â-pinene photooxidation by OH in the atmosphere simulation chamber SAPHIR, Atmos. Chem. Phys., 17, 6631–6650, https://doi.org/10.5194/acp-17-6631-2017, 2017.

Kanaya, Y., Cao, R., Akimoto, H., Fukuda, M., Komazaki, Y., Yokouchi, Y., Koike, M., Tanimoto, H., Takegawa, N., and Kondo, Y.: Urban photochemistry in central Tokyo: 1. Observed and modeled OH and HO$_2$ radical concentrations during the winter and summer of 2004, J. Geophys. Res.-Atmos., 112, D21312, https://doi.org/10.1029/2007jd008670, 2007.

Kanaya, Y., Hofzumahaus, A., Dorn, H. P., Brauers, T., Fuchs, H., Holland, F., Rohrer, F., Bohn, B., Tillmann, R., Wegener, R., Wahner, A., Kajii, Y., Miyamoto, K., Nishida, S., Watanabe, K., Yoshino, A., Kubistin, D., Martinez, M., Rudolf, M., Harder, H., Berresheim, H., Elste, T., Plass-Dülmer, C., Stange, G., Kleffmann, J., Elshorbany, Y., and Schurath, U.: Comparisons of observed and modeled OH and HO$_2$ concentrations during the ambient measurement period of the HO$_x$ Comp field campaign, Atmos. Chem. Phys., 12, 2567–2585, https://doi.org/10.5194/acp-12-2567-2012, 2012.

Kim, S., Wolfe, G. M., Mauldin, L., Cantrell, C., Guenther, A., Karl, T., Turnipseed, A., Greenberg, J., Hall, S. R., Ullmann, K., Apel, E., Hornbrook, R., Kajii, Y., Nakashima, Y., Keutsch, F. N., DiGangi, J. P., Henry, S. B., Kaser, L., Schnitzhofer, R., Graus, M., Hansel, A., Zheng, W., and Flocke, F. F.: Evaluation of HO$_x$ sources and cycling using measurement-constrained model calculations in a 2-methyl-3-butene-2-ol (MBO) and monoterpene (MT) dominated ecosystem, Atmos. Chem. Phys., 13, 2031–2044, https://doi.org/10.5194/acp-13-2031-2013, 2013.

Kleffmann, J., Lörzer, J. C., Wiesen, P., Kern, C., Trick, S., Volkamer, R., Rodenas, M., and Wirtz, K.: Intercomparison of the DOAS and LOPAP techniques for the detection of nitrous acid (HONO), Atmos. Environ., 40, 3640–3652, https://doi.org/10.1016/j.atmosenv.2006.03.027, 2006.

Kleinman, L. I., Daum, P. H., Lee, Y.-N., Nunnermacker, L. J., Springston, S. R., Weinstein-Lloyd, J., and Rudolph, J.: Ozone production efficiency in an urban area, J. Geophys. Res.-Atmos., 107, 4733, https://doi.org/10.1029/2002JD002529, 2002.

Komenda, M., Schaub, A., and Koppmann, R.: Description and characterization of an on-line system for long-term measurements of isoprene, methyl vinyl ketone, and methacrolein in ambient air, J. Chromatogr. A, 995, 185–201, https://doi.org/10.1016/S0021-9673(03)00518-1, 2003.

Konrad, S., Schmitz, T., Buers, H.-J., Houben, N., Mannschreck, K., Mihelcic, D., Müsgen, P., Pätz, H.-W., Holland, F., Hofzumahaus, A., Schäfer, H.-J., Schröder, S., Volz-Thomas, A., Bächmann, K., Schlomski, S., Moortgat, G., and Großmann, D.: Hydrocarbon measurements at Pabstthum during the BERLIOZ campaign and modeling of free radicals, J. Geophys. Res.-Atmos., 108, 8251, https://doi.org/10.1029/2001JD000866, 2003.

Kubistin, D., Harder, H., Martinez, M., Rudolf, M., Sander, R., Bozem, H., Eerdekens, G., Fischer, H., Gurk, C., Klüpfel, T., Königstedt, R., Parchatka, U., Schiller, C. L., Stickler, A., Taraborrelli, D., Williams, J., and Lelieveld, J.: Hydroxyl radicals in the tropical troposphere over the Suriname rainforest: comparison of measurements with the box model MECCA, Atmos. Chem. Phys., 10, 9705–9728, https://doi.org/10.5194/acp-10-9705-2010, 2010.

Lakey, P. S. J., George, I. J., Whalley, L. K., Baeza-Romero, M. T., and Heard, D. E.: Measurements of the HO$_2$ Uptake Coefficients onto Single Component Organic Aerosols, Environ. Sci. Technol., 49, 4878–4885, https://doi.org/10.1021/acs.est.5b00948, 2015.

Lelieveld, J., Butler, T. M., Crowley, J. N., Dillon, T. J., Fischer, H., Ganzeveld, L., Harder, H., Lawrence, M. G., Martinez, M., Taraborrelli, D., and Williams, J.: Atmospheric oxidation capacity sustained by a tropical forest, Nature, 452, 737–740, https://doi.org/10.1038/nature06870, 2008.

Lou, S., Holland, F., Rohrer, F., Lu, K., Bohn, B., Brauers, T., Chang, C. C., Fuchs, H., Häseler, R., Kita, K., Kondo, Y., Li, X., Shao, M., Zeng, L., Wahner, A., Zhang, Y., Wang, W., and Hofzumahaus, A.: Atmospheric OH reactivities in the Pearl River Delta – China in summer 2006: measurement and model results, Atmos. Chem. Phys., 10, 11243–11260, https://doi.org/10.5194/acp-10-11243-2010, 2010.

Lu, K. D., Hofzumahaus, A., Holland, F., Bohn, B., Brauers, T., Fuchs, H., Hu, M., Häseler, R., Kita, K., Kondo, Y., Li, X., Lou, S. R., Oebel, A., Shao, M., Zeng, L. M., Wahner, A., Zhu, T., Zhang, Y. H., and Rohrer, F.: Missing OH source in a suburban environment near Beijing: observed and modelled OH and HO$_2$ concentrations in summer 2006, Atmos. Chem. Phys., 13, 1057–1080, https://doi.org/10.5194/acp-13-1057-2013, 2013.

Lu, K. D., Rohrer, F., Holland, F., Fuchs, H., Brauers, T., Oebel, A., Dlugi, R., Hu, M., Li, X., Lou, S. R., Shao, M., Zhu, T., Wahner, A., Zhang, Y. H., and Hofzumahaus, A.: Nighttime observation and chemistry of HO$_X$ in the Pearl River Delta and Beijing in summer 2006, Atmos. Chem. Phys., 14, 4979–4999, https://doi.org/10.5194/acp-14-4979-2014, 2014.

Ma, X., Tan, Z., Lu, K., Yang, X., Liu, Y., Li, S., Li, X., Chen, S., Novelli, A., Cho, C., Zeng, L., Wahner, A., and Zhang, Y.: Winter photochemistry in Beijing: Observation and model simulation of

OH and HO$_2$ radicals at an urban site, Sci. Tot. Environ., 685, 85–95, https://doi.org/10.1016/j.scitotenv.2019.05.329, 2019.

Malkin, T. L., Goddard, A., Heard, D. E., and Seakins, P. W.: Measurements of OH and HO$_2$ yields from the gas phase ozonolysis of isoprene, Atmos. Chem. Phys., 10, 1441–1459, https://doi.org/10.5194/acp-10-1441-2010, 2010.

Mao, J., Ren, X., Chen, S., Brune, W. H., Chen, Z., Martinez, M., Harder, H., Lefer, B., Rappenglück, B., Flynn, J., and Leuchner, M.: Atmospheric oxidation capacity in the summer of Houston 2006: Comparison with summer measurements in other metropolitan studies, Atmos. Environ., 44, 4107–4115, https://doi.org/10.1016/j.atmosenv.2009.01.013, 2010.

Mao, J., Ren, X., Zhang, L., Van Duin, D. M., Cohen, R. C., Park, J. H., Goldstein, A. H., Paulot, F., Beaver, M. R., Crounse, J. D., Wennberg, P. O., DiGangi, J. P., Henry, S. B., Keutsch, F. N., Park, C., Schade, G. W., Wolfe, G. M., Thornton, J. A., and Brune, W. H.: Insights into hydroxyl measurements and atmospheric oxidation in a California forest, Atmos. Chem. Phys., 12, 8009–8020, https://doi.org/10.5194/acp-12-8009-2012, 2012.

Martinez, M., Harder, H., Kovacs, T. A., Simpas, J. B., Bassis, J., Lesher, R., Brune, W. H., Frost, G. J., Williams, E. J., Stroud, C. A., Jobson, B. T., Roberts, J. M., Hall, S. R., Shetter, R. E., Wert, B., Fried, A., Alicke, B., Stutz, J., Young, V. L., White, A. B., and Zamora, R. J.: OH and HO$_2$ concentrations, sources, and loss rates during the Southern Oxidants Study in Nashville, Tennessee, summer 1999, J. Geophys. Res.-Atmos., 108, 4617, https://doi.org/10.1029/2003JD003551, 2003.

Mihelcic, D., Holland, F., Hofzumahaus, A., Hoppe, L., Konrad, S., Müsgen, P., Pätz, H.-W., Schäfer, H.-J., Schmitz, T., Volz-Thomas, A., Bächmann, K., Schlomski, S., Platt, U., Geyer, A., Alicke, B., and Moortgat, G. K.: Peroxy radicals during BERLIOZ at Pabstthum: Measurements, radical budgets and ozone production, J. Geophys. Res.-Atmos., 108, D4, https://doi.org/10.1029/2001JD001014, 2003.

Nehr, S., Bohn, B., Fuchs, H., Hofzumahaus, A., and Wahner, A.: HO$_2$ formation from the OH$^+$ benzene reaction in the presence of O$_2$, Phys. Chem. Chem. Phys., 13, 10699–10708, https://doi.org/10.1039/C1CP20334G, 2011.

Nehr, S., Bohn, B., Dorn, H. P., Fuchs, H., Häseler, R., Hofzumahaus, A., Li, X., Rohrer, F., Tillmann, R., and Wahner, A.: Atmospheric photochemistry of aromatic hydrocarbons: OH budgets during SAPHIR chamber experiments, Atmos. Chem. Phys., 14, 6941–6952, https://doi.org/10.5194/acp-14-6941-2014, 2014.

Novelli, A., Hens, K., Tatum Ernest, C., Kubistin, D., Regelin, E., Elste, T., Plass-Dülmer, C., Martinez, M., Lelieveld, J., and Harder, H.: Characterisation of an inlet pre-injector laser-induced fluorescence instrument for the measurement of atmospheric hydroxyl radicals, Atmos. Meas. Tech., 7, 3413–3430, https://doi.org/10.5194/amt-7-3413-2014, 2014.

Novelli, A., Kaminski, M., Rolletter, M., Acir, I. H., Bohn, B., Dorn, H. P., Li, X., Lutz, A., Nehr, S., Rohrer, F., Tillmann, R., Wegener, R., Holland, F., Hofzumahaus, A., Kiendler-Scharr, A., Wahner, A., and Fuchs, H.: Evaluation of OH and HO$_2$ concentrations and their budgets during photooxidation of 2-methyl-3-butene-2-ol (MBO) in the atmospheric simulation chamber SAPHIR, Atmos. Chem. Phys., 18, 11409–11422, https://doi.org/10.5194/acp-18-11409-2018, 2018.

Novelli, A., Vereecken, L., Bohn, B., Dorn, H. P., Gkatzelis, G. I., Hofzumahaus, A., Holland, F., Reimer, D., Rohrer, F., Rosanka, S., Taraborrelli, D., Tillmann, R., Wegener, R., Yu, Z., Kiendler-Scharr, A., Wahner, A., and Fuchs, H.: Importance of isomerization reactions for OH radical regeneration from the photo-oxidation of isoprene investigated in the atmospheric simulation chamber SAPHIR, Atmos. Chem. Phys., 20, 3333–3355, https://doi.org/10.5194/acp-20-3333-2020, 2020.

Novelli, A., Cho, C., Fuchs, H., Hofzumahaus, A., Rohrer, F., Tillmann, R., Kiendler-Scharr, A., Wahner, A., and Vereecken, L.: Experimental and theoretical study on the impact of a nitrate group on the chemistry of alkoxy radicals, Phys. Chem. Chem. Phys., 23, 5474–5495, https://doi.org/10.1039/d0cp05555g, 2021.

Osthoff, H. D., Roberts, J. M., Ravishankara, A. R., Williams, E. J., Lerner, B. M., Sommariva, R., Bates, T. S., Coffman, D., Quinn, P. K., Dibb, J. E., Stark, H., Burkholder, J. B., Talukdar, R. K., Meagher, J., Fehsenfeld, F. C., and Brown, S. S.: High levels of nitryl chloride in the polluted subtropical marine boundary layer, Nat. Geosci., 1, 324–328, https://doi.org/10.1038/ngeo177, 2008.

Peeters, J. and Müller, J.-F.: HO$_x$ radical regeneration in isoprene oxidation via peroxy radical isomerisations, II: experimental evidence and global impact, Phys. Chem. Chem. Phys., 12, 14227–14235, https://doi.org/10.1039/C0CP00811G, 2010.

Peeters, J., Nguyen, T., and Vereecken, L.: HO$_x$ radical regeneration in the oxidation of isoprene, Phys. Chem. Chem. Phys, 11, 5935–5939, https://doi.org/10.1039/b908511d, 2009.

Peeters, J., Müller, J. F., Stavrakou, T., and Vinh Son, N.: Hydroxyl radical recycling in isoprene oxidation driven by hydrogen bonding and hydrogen tunneling: The upgraded LIM1 mechanism, J. Phys. Chem.. A, 118, 8625–8643, https://doi.org/10.1021/jp5033146, 2014.

Praske, E., Crounse, J. D., Bates, K. H., Kurtén, T., Kjaergaard, H. G., and Wennberg, P. O.: Atmospheric Fate of Methyl Vinyl Ketone: Peroxy Radical Reactions with NO and HO$_2$, J. Phys. Chem. A, 119, 4562–4572, https://doi.org/10.1021/jp5107058, 2015.

Ren, X., Harder, H., Martinez, M., Lesher, R. L., Oliger, A., Simpas, J. B., Brune, W. H., Schwab, J. J., Demerjian, K. L., He, Y., Zhou, X., and Gao, H.: OH and HO$_2$ Chemistry in the urban atmosphere of New York City, Atmos. Environ., 37, 3639–3651, https://doi.org/10.1016/S1352-2310(03)00459-X, 2003.

Ren, X., Brune, W. H., Mao, J., Mitchell, M. J., Lesher, R. L., Simpas, J. B., Metcalf, A. R., Schwab, J. J., Cai, C., Li, Y., Demerjian, K. L., Felton, H. D., Boynton, G., Adams, A., Perry, J., He, Y., Zhou, X., and Hou, J.: Behavior of OH and HO$_2$ in the winter atmosphere in New York City, Atmos. Environ., 40, 252–263, https://doi.org/10.1016/j.atmosenv.2005.11.073, 2006.

Ren, X., van Duin, D., Cazorla, M., Chen, S., Mao, J., Zhang, L., Brune, W. H., Flynn, J. H., Grossberg, N., Lefer, B. L., Rappenglück, B., Wong, K. W., Tsai, C., Stutz, J., Dibb, J. E., Thomas Jobson, B., Luke, W. T., and Kelley, P.: Atmospheric oxidation chemistry and ozone production: Results from SHARP 2009 in Houston, Texas, J. Geophys. Res.-Atmos., 118, 5770–5780, https://doi.org/10.1002/jgrd.50342, 2013.

Rhew, R. C., Deventer, M. J., Turnipseed, A. A., Warneke, C., Ortega, J., Shen, S., Martinez, L., Koss, A., Lerner, B. M., Gilman, J. B., Smith, J. N., Guenther, A. B., and de Gouw, J. A.: Ethene,

propene, butene and isoprene emissions from a ponderosa pine forest measured by relaxed eddy accumulation, Atmos. Chem. Phys., 17, 13417–13438, https://doi.org/10.5194/acp-17-13417-2017, 2017.

Rohrer, F., Bohn, B., Brauers, T., Brüning, D., Johnen, F. J., Wahner, A., and Kleffmann, J.: Characterisation of the photolytic HONO-source in the atmosphere simulation chamber SAPHIR, Atmos. Chem. Phys., 5, 2189–2201, https://doi.org/10.5194/acp-5-2189-2005, 2005.

Rohrer, F., Lu, K., Hofzumahaus, A., Bohn, B., Brauers, T., Chang, C.-C., Fuchs, H., Häseler, R., Holland, F., Hu, M., Kita, K., Kondo, Y., Li, X., Lou, S., Oebel, A., Shao, M., Zeng, L., Zhu, T., Zhang, Y., and Wahner, A.: Maximum efficiency in the hydroxyl-radical-based self-cleansing of the troposphere, Nat. Geosci., 7, 559–563, https://doi.org/10.1038/ngeo2199, 2014.

Rolletter, M., Kaminski, M., Acir, I. H., Bohn, B., Dorn, H. P., Li, X., Lutz, A., Nehr, S., Rohrer, F., Tillmann, R., Wegener, R., Hofzumahaus, A., Kiendler-Scharr, A., Wahner, A., and Fuchs, H.: Investigation of the á-pinene photooxidation by OH in the atmospheric simulation chamber SAPHIR, Atmos. Chem. Phys., 19, 11635–11649, https://doi.org/10.5194/acp-19-11635-2019, 2019.

Rolletter, M., Blocquet, M., Kaminski, M., Bohn, B., Dorn, H. P., Hofzumahaus, A., Holland, F., Li, X., Rohrer, F., Tillmann, R., Wegener, R., Kiendler-Scharr, A., Wahner, A., and Fuchs, H.: Photooxidation of pinonaldehyde at ambient conditions investigated in the atmospheric simulation chamber SAPHIR, Atmos. Chem. Phys., 20, 13701–13719, https://doi.org/10.5194/acp-20-13701-2020, 2020.

Schlosser, E., Bohn, B., Brauers, T., Dorn, H.-P., Fuchs, H., Häseler, R., Hofzumahaus, A., Holland, F., Rohrer, F., Rupp, L. O., Siese, M., Tillmann, R., and Wahner, A.: Intercomparison of two hydroxyl radical measurement techniques at the atmosphere simulation chamber SAPHIR, J. Atmos. Chem., 56, 187–205, https://doi.org/10.1007/s10874-006-9049-3, 2007.

Schlosser, E., Brauers, T., Dorn, H. P., Fuchs, H., Häseler, R., Hofzumahaus, A., Holland, F., Wahner, A., Kanaya, Y., Kajii, Y., Miyamoto, K., Nishida, S., Watanabe, K., Yoshino, A., Kubistin, D., Martinez, M., Rudolf, M., Harder, H., Berresheim, H., Elste, T., Plass-Dülmer, C., Stange, G., and Schurath, U.: Technical Note: Formal blind intercomparison of OH measurements: results from the international campaign HOxComp, Atmos. Chem. Phys., 9, 7923–7948, https://doi.org/10.5194/acp-9-7923-2009, 2009.

Sarkar, C., Guenther, A. B., Park, J. H., Seco, R., Alves, E., Batalha, S., Santana, R., Kim, S., Smith, J., Tóta, J., and Vega, O.: PTR-TOF-MS eddy covariance measurements of isoprene and monoterpene fluxes from an eastern Amazonian rainforest, Atmos. Chem. Phys., 20, 7179–7191, https://doi.org/10.5194/acp-20-7179-2020, 2020.

Sillman, S., Logan, J. A., and Wofsy, S. C.: The sensitivity of ozone to nitrogen oxides and hydrocarbons in regional ozone episodes, J. Geophys. Res.-Atmos., 95, 1837–1851, https://doi.org/10.1029/JD095iD02p01837, 1990.

Slater, E. J., Whalley, L. K., Woodward-Massey, R., Ye, C., Lee, J. D., Squires, F., Hopkins, J. R., Dunmore, R. E., Shaw, M., Hamilton, J. F., Lewis, A. C., Crilley, L. R., Kramer, L., Bloss, W., Vu, T., Sun, Y., Xu, W., Yue, S., Ren, L., Acton, W. J. F., Hewitt, C. N., Wang, X., Fu, P., and Heard, D. E.: El-

evated levels of OH observed in haze events during wintertime in central Beijing, Atmos. Chem. Phys., 20, 14847–14871, https://doi.org/10.5194/acp-20-14847-2020, 2020.

Sommariva, R., Bloss, W. J., Brough, N., Carslaw, N., Flynn, M., Haggerstone, A. L., Heard, D. E., Hopkins, J. R., Lee, J. D., Lewis, A. C., McFiggans, G., Monks, P. S., Penkett, S. A., Pilling, M. J., Plane, J. M. C., Read, K. A., Saiz-Lopez, A., Rickard, A. R., and Williams, P. I.: OH and HO$_2$ chemistry during NAMBLEX: roles of oxygenates, halogen oxides and heterogeneous uptake, Atmos. Chem. Phys., 6, 1135–1153, https://doi.org/10.5194/acp-6-1135-2006, 2006.

Sommariva, R., Hollis, L. D. J., Sherwen, T., Baker, A. R., Ball, S. M., Bandy, B. J., Bell, T. G., Chowdhury, M. N., Cordell, R. L., Evans, M. J., Lee, J. D., Reed, C., Reeves, C. E., Roberts, J. M., Yang, M., and Monks, P. S.: Seasonal and geographical variability of nitryl chloride and its precursors in Northern Europe, Atmos. Sci. Lett., 19, UNSP e844, https://doi.org/10.1002/asl.844, 2018.

Song, H., Chen, X., Lu, K., Zou, Q., Tan, Z., Fuchs, H., Wiedensohler, A., Moon, D. R., Heard, D. E., Baeza-Romero, M. T., Zheng, M., Wahner, A., Kiendler-Scharr, A., and Zhang, Y.: Influence of aerosol copper on HO$_2$ uptake: a novel parameterized equation, Atmos. Chem. Phys., 20, 15835–15850, https://doi.org/10.5194/acp-20-15835-2020, 2020.

Spirig, C., Neftel, A., Ammann, C., Dommen, J., Grabmer, W., Thielmann, A., Schaub, A., Beauchamp, J., Wisthaler, A., and Hansel, A.: Eddy covariance flux measurements of biogenic VOCs during ECHO 2003 using proton transfer reaction mass spectrometry, Atmos. Chem. Phys., 5, 465–481, https://doi.org/10.5194/acp-5-465-2005, 2005.

Stone, D., Whalley, L. K., and Heard, D. E.: Tropospheric OH and HO$_2$ radicals: field measurements and model comparisons, Chem. Soc. Rev., 41, 6348–6404, https://doi.org/10.1039/C2CS35140D, 2012.

Stone, D., Sherwen, T., Evans, M. J., Vaughan, S., Ingham, T., Whalley, L. K., Edwards, P. M., Read, K. A., Lee, J. D., Moller, S. J., Carpenter, L. J., Lewis, A. C., and Heard, D. E.: Impacts of bromine and iodine chemistry on tropospheric OH and HO$_2$: comparing observations with box and global model perspectives, Atmos. Chem. Phys., 18, 3541–3561, https://doi.org/10.5194/acp-18-3541-2018, 2018.

Taketani, F., Kanaya, Y., and Akimoto, H.: Kinetics of Heterogeneous Reactions of HO$_2$ Radical at Ambient Concentration Levels with (NH$_4$)2SO$_4$ and NaCl Aerosol Particles, J. Phys. Chem.. A, 112, 2370–2377, https://doi.org/10.1021/jp0769936, 2008.

Taketani, F., Kanaya, Y., and Akimoto, H.: Heterogeneous loss of HO$_2$ by KCl, synthetic sea salt, and natural seawater aerosol particles, Atmos. Environ., 43, 1660–1665, https://doi.org/10.1016/j.atmosenv.2008.12.010, 2009.

Tan, D., Faloona, I., Simpas, J. B., Brune, W., Shepson, P. B., Couch, T. L., Sumner, A. L., Carroll, M. A., Thornberry, T., Apel, E., Riemer, D., and Stockwell, W.: HO$_x$ budgets in a deciduous forest: Results from the PROPHET summer 1998 campaign, J. Geophys. Res.-Atmos., 106, 24407–24427, https://doi.org/10.1029/2001jd900016, 2001.

Tan, Z., Fuchs, H., Lu, K., Hofzumahaus, A., Bohn, B., Broch, S., Dong, H., Gomm, S., Häseler, R., He, L., Holland, F., Li, X., Liu, Y., Lu, S., Rohrer, F., Shao, M., Wang, B., Wang, M., Wu, Y., Zeng, L., Zhang, Y., Wahner, A., and Zhang, Y.: Radical chem-

istry at a rural site (Wangdu) in the North China Plain: observation and model calculations of OH, HO$_2$ and RO$_2$ radicals, Atmos. Chem. Phys., 17, 663–690, https://doi.org/10.5194/acp-17-663-2017, 2017.

Tan, Z., Rohrer, F., Lu, K., Ma, X., Bohn, B., Broch, S., Dong, H., Fuchs, H., Gkatzelis, G. I., Hofzumahaus, A., Holland, F., Li, X., Liu, Y., Liu, Y., Novelli, A., Shao, M., Wang, H., Wu, Y., Zeng, L., Hu, M., Kiendler-Scharr, A., Wahner, A., and Zhang, Y.: Wintertime photochemistry in Beijing: observations of ROx radical concentrations in the North China Plain during the BEST-ONE campaign, Atmos. Chem. Phys., 18, 12391–12411, https://doi.org/10.5194/acp-18-12391-2018, 2018.

Tan, Z., Lu, K., Hofzumahaus, A., Fuchs, H., Bohn, B., Holland, F., Liu, Y., Rohrer, F., Shao, M., Sun, K., Wu, Y., Zeng, L., Zhang, Y., Zou, Q., Kiendler-Scharr, A., Wahner, A., and Zhang, Y.: Experimental budgets of OH, HO$_2$, and RO$_2$ radicals and implications for ozone formation in the Pearl River Delta in China 2014, Atmos. Chem. Phys., 19, 7129–7150, https://doi.org/10.5194/acp-19-7129-2019, 2019.

Tan, Z., Hofzumahaus, A., Lu, K., Brown, S. S., Holland, F., Huey, L. G., Kiendler-Scharr, A., Li, X., Liu, X., Ma, N., Min, K.-E., Rohrer, F., Shao, M., Wahner, A., Wang, Y., Wiedensohler, A., Wu, Y., Wu, Z., Zeng, L., Zhang, Y., and Fuchs, H.: No Evidence for a Significant Impact of Heterogeneous Chemistry on Radical Concentrations in the North China Plain in Summer 2014, Environ. Sci. Technol., 54, 5973–5979, https://doi.org/10.1021/acs.est.0c00525, 2020.

Tan, Z., Fuchs, H., Hofzumahaus, A., Bloss, W. J., Bohn, B., Cho, C., Hohaus, T., Holland, F., Lakshmisha, C., Liu, L., Monks, P. S., Novelli, A., Niether, D., Rohrer, F., Tillmann, R., Valkenburg, T. S. E., Vardhan, V., Kiendler-Scharr, A., Wahner, A., and Sommariva, R.: Seasonal variation in nitryl chloride and its relation to gas-phase precursors during the JULIAC campaign in Germany, Atmos. Chem. Phys., 22, 13137–13152, https://doi.org/10.5194/acp-22-13137-2022, 2022.

Tanaka, P. L., Riemer, D. D., Chang, S., Yarwood, G., McDonald-Buller, E. C., Apel, E. C., Orlando, J. J., Silva, P. J., Jimenez, J. L., Canagaratna, M. R., Neece, J. D., Mullins, C. B., and Allen, D. T.: Direct evidence for chlorine-enhanced urban ozone formation in Houston, Texas, Atmos. Environ., 37, 1393–1400, https://doi.org/10.1016/S1352-2310(02)01007-5, 2003.

Teng, A. P., Crounse, J. D., and Wennberg, P. O.: Isoprene peroxy radical dynamics, J. Am. Chem. Soc., 139, 5367–5377, https://doi.org/10.1021/jacs.6b12838, 2017.

Thornton, J. A., Kercher, J. P., Riedel, T. P., Wagner, N. L., Cozic, J., Holloway, J. S., Dubé, W. P., Wolfe, G. M., Quinn, P. K., Middlebrook, A. M., Alexander, B., and Brown, S. S.: A large atomic chlorine source inferred from mid-continental reactive nitrogen chemistry, Nature, 464, 271–274, https://doi.org/10.1038/nature08905, 2010.

Vaughan, S., Ingham, T., Whalley, L. K., Stone, D., Evans, M. J., Read, K. A., Lee, J. D., Moller, S. J., Carpenter, L. J., Lewis, A. C., Fleming, Z. L., and Heard, D. E.: Seasonal observations of OH and HO$_2$ in the remote tropical marine boundary layer, Atmos. Chem. Phys., 12, 2149–2172, https://doi.org/10.5194/acp-12-2149-2012, 2012.

Vilà-Guerau de Arellano, J., van den Dries, K., and Pino, D.: On inferring isoprene emission surface flux from atmospheric boundary layer concentration measurements, Atmos. Chem. Phys., 9, 3629–3640, https://doi.org/10.5194/acp-9-3629-2009, 2009.

Wang, F., Hu, R., Chen, H., Xie, P., Wang, Y., Li, Z., Jin, H., Liu, J., and Liu, W.: Development of a field system for measurement of tropospheric OH radical using laser-induced fluorescence technique, Optics Express, 27, 419–435, https://doi.org/10.1364/OE.27.00A419, 2019.

Whalley, L. K., Edwards, P. M., Furneaux, K. L., Goddard, A., Ingham, T., Evans, M. J., Stone, D., Hopkins, J. R., Jones, C. E., Karunaharan, A., Lee, J. D., Lewis, A. C., Monks, P. S., Moller, S. J., and Heard, D. E.: Quantifying the magnitude of a missing hydroxyl radical source in a tropical rainforest, Atmos. Chem. Phys., 11, 7223–7233, https://doi.org/10.5194/acp-11-7223-2011, 2011.

Whalley, L. K., Stone, D., Dunmore, R., Hamilton, J., Hopkins, J. R., Lee, J. D., Lewis, A. C., Williams, P., Kleffmann, J., Laufs, S., Woodward-Massey, R., and Heard, D. E.: Understanding in situ ozone production in the summertime through radical observations and modelling studies during the Clean air for London project (ClearfLo), Atmos. Chem. Phys., 18, 2547–2571, https://doi.org/10.5194/acp-18-2547-2018, 2018.

Whalley, L. K., Slater, E. J., Woodward-Massey, R., Ye, C., Lee, J. D., Squires, F., Hopkins, J. R., Dunmore, R. E., Shaw, M., Hamilton, J. F., Lewis, A. C., Mehra, A., Worrall, S. D., Bacak, A., Bannan, T. J., Coe, H., Percival, C. J., Ouyang, B., Jones, R. L., Crilley, L. R., Kramer, L. J., Bloss, W. J., Vu, T., Kotthaus, S., Grimmond, S., Sun, Y., Xu, W., Yue, S., Ren, L., Acton, W. J. F., Hewitt, C. N., Wang, X., Fu, P., and Heard, D. E.: Evaluating the sensitivity of radical chemistry and ozone formation to ambient VOCs and NO$_x$ in Beijing, Atmos. Chem. Phys., 21, 2125–2147, https://doi.org/10.5194/acp-21-2125-2021, 2021.

Winiberg, F. A. F., Dillon, T. J., Orr, S. C., Groß, C. B. M., Bejan, I., Brumby, C. A., Evans, M. J., Smith, S. C., Heard, D. E., and Seakins, P. W.: Direct measurements of OH and other product yields from the HO$_2$ + CH$_3$C(O)O$_2$ reaction, Atmos. Chem. Phys., 16, 4023–4042, https://doi.org/10.5194/acp-16-4023-2016, 2016.

Wolfe, G. M., Thornton, J. A., Bouvier-Brown, N. C., Goldstein, A. H., Park, J. H., McKay, M., Matross, D. M., Mao, J., Brune, W. H., LaFranchi, B. W., Browne, E. C., Min, K. E., Wooldridge, P. J., Cohen, R. C., Crounse, J. D., Faloona, I. C., Gilman, J. B., Kuster, W. C., de Gouw, J. A., Huisman, A., and Keutsch, F. N.: The Chemistry of Atmosphere-Forest Exchange (CAFE) Model – Part 2: Application to BEARPEX-2007 observations, Atmos. Chem. Phys., 11, 1269–1294, https://doi.org/10.5194/acp-11-1269-2011, 2011.

Wolfe, G. M., Cantrell, C., Kim, S., Mauldin Iii, R. L., Karl, T., Harley, P., Turnipseed, A., Zheng, W., Flocke, F., Apel, E. C., Hornbrook, R. S., Hall, S. R., Ullmann, K., Henry, S. B., DiGangi, J. P., Boyle, E. S., Kaser, L., Schnitzhofer, R., Hansel, A., Graus, M., Nakashima, Y., Kajii, Y., Guenther, A., and Keutsch, F. N.: Missing peroxy radical sources within a summertime ponderosa pine forest, Atmos. Chem. Phys., 14, 4715–4732, https://doi.org/10.5194/acp-14-4715-2014, 2014.